2024-2025

THÈSE

pour le

DIPLÔME D'ÉTAT DE DOCTEUR EN MÉDECINE

Qualification en D.E.S. de Médecine nucléaire

Ergonomics and artificial intelligence in PET imaging: Impact of user interfaces on diagnostic performance

Ergonomie et intelligence artificielle en imagerie TEP : Impact des interfaces utilisateur sur la performance diagnostique

Study 1 **– Value of artificial intelligence in reducing PET image acquisition time: routine clinical validation using qualitative, quantitative, and radiomic analysis on a cohort of 282 patients undergoing [^{18}F]FDG and [^{68}Ga]PSMA PET/CT**

Study 2 **– Innovative Evaluation of a Non-Conventional Mouse for Image Interpretation in Metabolic Imaging: Integration of Eye Tracking, Kinematic Analysis, and Qualitative Feedback**

DAMBRAIN Abel
Né le 19/08/1998 à Royan (17)

Sous la direction du Docteur BOURON Clément

Membres du jury

Monsieur le Professeur LACOEUILLE Franck	Président
Monsieur le Docteur BOURON Clément	Directeur
Monsieur le Docteur GONTIER Éric	Membre
Madame le Docteur GIRAULT Sylvie	Membre
Madame le Docteur GUILLERMINET Camille	Membre (invité)
Madame le Docteur CAVARO-MENARD Christine	Membre (invité)

Soutenue publiquement le : 24/10/2025
A Angers

FACULTÉ DE SANTÉ
UNIVERSITÉ D'ANGERS

ENGAGEMENT DE NON PLAGIAT

Je, soussigné DAMBRAIN Abel
déclare être pleinement conscient que le plagiat de documents ou d'une partie d'un document publiée sur toutes formes de support, y compris l'internet, constitue une violation des droits d'auteur ainsi qu'une fraude caractérisée.
En conséquence, je m'engage à citer toutes les sources que j'ai utilisées pour écrire ce rapport ou mémoire.

Signé par l'étudiant le **23/09/2025**

SERMENT D'HIPPOCRATE

« Au moment d'être admis à exercer la médecine, je promets et je jure d'être fidèle aux lois de l'honneur et de la probité. Mon premier souci sera de rétablir, de préserver ou de promouvoir la santé dans tous ses éléments, physiques et mentaux, individuels et sociaux. Je respecterai toutes les personnes, leur autonomie et leur volonté, sans aucune discrimination selon leur état ou leurs convictions. J'interviendrai pour les protéger si elles sont affaiblies, vulnérables ou menacées dans leur intégrité ou leur dignité. Même sous la contrainte, je ne ferai pas usage de mes connaissances contre les lois de l'humanité. J'informerai les patients des décisions envisagées, de leurs raisons et de leurs conséquences. Je ne tromperai jamais leur confiance et n'exploiterai pas le pouvoir hérité des circonstances pour forcer les consciences. Je donnerai mes soins à l'indigent et à quiconque me les demandera. Je ne me laisserai pas influencer par la soif du gain ou la recherche de la gloire.

Admis dans l'intimité des personnes, je tairai les secrets qui me seront confiés. Reçu à l'intérieur des maisons, je respecterai les secrets des foyers et ma conduite ne servira pas à corrompre les mœurs. Je ferai tout pour soulager les souffrances. Je ne prolongerai pas abusivement les agonies. Je ne provoquerai jamais la mort délibérément.

Je préserverai l'indépendance nécessaire à l'accomplissement de ma mission. Je n'entreprendrai rien qui dépasse mes compétences. Je les entretiendrai et les perfectionnerai pour assurer au mieux les services qui me seront demandés.

J'apporterai mon aide à mes confrères ainsi qu'à leurs familles dans l'adversité. Que les hommes et mes confrères m'accordent leur estime si je suis fidèle à mes promesses ; que je sois déshonoré et méprisé si j'y manque ».

LISTE DES ENSEIGNANTS DE LA FACULTÉ DE SANTÉ D'ANGERS

Doyen de la Faculté : Pr Cédric ANNWEILER
Vice-Doyen de la Faculté et directeur du département de pharmacie : Pr Sébastien FAURE
Directeur du département de médecine : Pr Vincent DUBEE

PROFESSEURS DES UNIVERSITÉS

ABRAHAM Pierre	PHYSIOLOGIE	Médecine
ANGOULVANT Cécile	MEDECINE GENERALE	Médecine
ANNWEILER Cédric	GERIATRIE ET BIOLOGIE DU VIEILLISSEMENT	Médecine
ASFAR Pierre	REANIMATION	Médecine
AUBE Christophe	RADIOLOGIE ET IMAGERIE MEDICALE	Médecine
AUGUSTO Jean-François	NEPHROLOGIE	Médecine
BAUFRETON Christophe	CHIRURGIE THORACIQUE ET CARDIOVASCULAIRE	Médecine
BELLANGER William	MEDECINE GENERALE	Médecine
BELONCLE François	REANIMATION	Médecine
BIERE Loïc	CARDIOLOGIE	Médecine
BIGOT Pierre	UROLOGIE	Médecine
BONNEAU Dominique	GENETIQUE	Médecine
BOUCHARA Jean-Philippe	PARASITOLOGIE ET MYCOLOGIE	Médecine
BOUET Pierre-Emmanuel	GYNECOLOGIE-OBSTETRIQUE	Médecine
BOURSIER Jérôme	GASTROENTEROLOGIE ; HEPATOLOGIE	Médecine
BOUVARD Béatrice	RHUMATOLOGIE	Médecine
BRIET Marie	PHARMACOLOGIE	Médecine
CAMPONE Mario	CANCEROLOGIE ; RADIOTHERAPIE	Médecine
CAROLI-BOSC François-Xavier	GASTROENTEROLOGIE ; HEPATOLOGIE	Médecine
CASSEREAU Julien	NEUROLOGIE	Médecine
CLERE Nicolas	PHARMACOLOGIE / PHYSIOLOGIE	Pharmacie
COLIN Estelle	GENETIQUE	Médecine
CONNAN Laurent	MEDECINE GENERALE	Médecine
COPIN Marie-Christine	ANATOMIE ET CYTOLOGIE PATHOLOGIQUES	Médecine
COUTANT Régis	PEDIATRIE	Médecine
CUSTAUD Marc-Antoine	PHYSIOLOGIE	Médecine
CRAUSTE-MANCIET Sylvie	PHARMACOTECHNIE HOSPITALIERE	Pharmacie
DE CASABIANCA Catherine	MEDECINE GENERALE	Médecine
DERBRE Séverine	PHARMACOGNOSIE	Pharmacie
DESCAMPS Philippe	GYNECOLOGIE-OBSTETRIQUE	Médecine
D'ESCATHA Alexis	MEDECINE ET SANTE AU TRAVAIL	Médecine

DINOMAIS Mickaël	MEDECINE PHYSIQUE ET DE READAPTATION	Médecine
DUBEE Vincent	MALADIES INFECTIEUSES ET TROPICALES	Médecine
DUCANCELLE Alexandra	BACTERIOLOGIE-VIROLOGIE ; HYGIENE HOSPITALIERE	Médecine
DUVERGER Philippe	PEDOPSYCHIATRIE	Médecine
EVEILLARD Matthieu	BACTERIOLOGIE-VIROLOGIE	Pharmacie
FAURE Sébastien	PHARMACOLOGIE PHYSIOLOGIE	Pharmacie
FOURNIER Henri-Dominique	ANATOMIE	Médecine
FOUQUET Olivier	CHIRURGIE THORACIQUE ET CARDIOVASCULAIRE	Médecine
FURBER Alain	CARDIOLOGIE	Médecine
GAGNADOUX Frédéric	PNEUMOLOGIE	Médecine
GOHIER Bénédicte	PSYCHIATRIE D'ADULTES	Médecine
GUARDIOLA Philippe	HEMATOLOGIE ; TRANSFUSION	Médecine
GUILET David	CHIMIE ANALYTIQUE	Pharmacie
HUNAULT-BERGER Mathilde	HEMATOLOGIE ; TRANSFUSION	Médecine
JEANNIN Pascale	IMMUNOLOGIE	Médecine
KAZOUR François	PSYCHIATRIE	Médecine
KEMPF Marie	BACTERIOLOGIE-VIROLOGIE ; HYGIENE HOSPITALIERE	Médecine
KUN-DARBOIS Daniel	CHIRURGIE MAXILLO-FACIALE ET STOMATOLOGIE	Médecine
LACOEUILLE FRANCK	RADIOPHARMACIE	Pharmacie
LACCOURREYE Laurent	OTO-RHINO-LARYNGOLOGIE	Médecine
LAGARCE Frédéric	BIOPHARMACIE	Pharmacie
LANDREAU Anne	BOTANIQUE/ MYCOLOGIE	Pharmacie
LASOCKI Sigismond	ANESTHESIOLOGIE-REANIMATION	Médecine
LEBDAI Souhil	UROLOGIE	Médecine
LEGENDRE Guillaume	GYNECOLOGIE-OBSTETRIQUE	Médecine
LEGRAND Erick	RHUMATOLOGIE	Médecine
LEMEE Jean-Michel	NEUROCHIRURGIE	Médecine
LERMITE Emilie	CHIRURGIE GENERALE	Médecine
LEROLLE Nicolas	REANIMATION	Médecine
LIBOUBAN Hélène	HISTOLOGIE	Médecine
LUQUE PAZ Damien	HEMATOLOGIE BIOLOGIQUE	Médecine
MARCHAIS Véronique	BACTERIOLOGIE-VIROLOGIE	Pharmacie
MARTIN Ludovic	DERMATO-VENEREOLOGIE	Médecine
MAY-PANLOUP Pascale	BIOLOGIE ET MEDECINE DU DEVELOPPEMENT ET DE LA REPRODUCTION	Médecine
MENEI Philippe	NEUROCHIRURGIE	Médecine
MERCAT Alain	REANIMATION	Médecine
ORVAIN Corentin	HEMATOLOGIE ; TRANSFUSION	Médecine
PAISANT Anita	RADIOLOGIE	Médecine
PAPON Nicolas	PARASITOLOGIE ET MYCOLOGIE MEDICALE	Pharmacie

PASSIRANI Catherine	CHIMIE GENERALE	Pharmacie
PELLIER Isabelle	PEDIATRIE	Médecine
PETIT Audrey	MEDECINE ET SANTE AU TRAVAIL	Médecine
PICQUET Jean	CHIRURGIE VASCULAIRE ; MEDECINE VASCULAIRE	Médecine
PODEVIN Guillaume	CHIRURGIE INFANTILE	Médecine
PROCACCIO Vincent	GENETIQUE	Médecine
PRUNIER Delphine	BIOCHIMIE ET BIOLOGIE MOLECULAIRE	Médecine
PRUNIER Fabrice	CARDIOLOGIE	Médecine
PY Thibaut	MEDECINE GENERALE	Médecine
RAMOND-ROQUIN Aline	MEDECINE GENERALE	Médecine
REYNIER Pascal	BIOCHIMIE ET BIOLOGIE MOLECULAIRE	Médecine
RIOU Jérémie	BIOSTATISTIQUE	Pharmacie
RINEAU Emmanuel	ANESTHESIOLOGIE REANIMATION	Médecine
RIQUIN Elise	PEDOPSYCHIATRIE ; ADDICTOLOGIE	Médecine
RODIEN Patrice	ENDOCRINOLOGIE, DIABETE ET MALADIES METABOLIQUES	Médecine
ROQUELAURE Yves	MEDECINE ET SANTE AU TRAVAIL	Médecine
ROUGE-MAILLART Clotilde	MEDECINE LEGALE ET DROIT DE LA SANTE	Médecine
ROUSSEAU Audrey	ANATOMIE ET CYTOLOGIE PATHOLOGIQUES	Médecine
ROUSSEAU Pascal	CHIRURGIE PLASTIQUE, RECONSTRUCTRICE ET ESTHETIQUE	Médecine
ROUSSELET Marie-Christine	ANATOMIE ET CYTOLOGIE PATHOLOGIQUES	Médecine
ROY Pierre-Marie	MEDECINE D'URGENCE	Médecine
SAULNIER Patrick	BIOPHYSIQUE ET BIOSTATISTIQUES	Pharmacie
SERAPHIN Denis	CHIMIE ORGANIQUE	Pharmacie
SCHMIDT Aline	HEMATOLOGIE ; TRANSFUSION	Médecine
TESSIER-CAZENEUVE Christine	MEDECINE GENERALE	Médecine
TRZEPIZUR Wojciech	PNEUMOLOGIE	Médecine
UGO Valérie	HEMATOLOGIE ; TRANSFUSION	Médecine
URBAN Thierry	PNEUMOLOGIE	Médecine
VAN BOGAERT Patrick	PEDIATRIE	Médecine
VENARA Aurélien	CHIRURGIE VISCERALE ET DIGESTIVE	Médecine
VENIER-JULIENNE Marie-Claire	PHARMACOTECHNIE	Pharmacie
VERNY Christophe	NEUROLOGIE	Médecine
WILLOTEAUX Serge	RADIOLOGIE ET IMAGERIE MEDICALE	Médecine

MAÎTRES DE CONFÉRENCES

AMMI Myriam	CHIRURGIE VASCULAIRE ET THORACIQUE	Médecine
BAGLIN Isabelle	CHIMIE THERAPEUTIQUE	Pharmacie

BASTIAT Guillaume	BIOPHYSIQUE ET BIOSTATISTIQUES	Pharmacie
BEAUVILLAIN Céline	IMMUNOLOGIE	Médecine
BEGUE Cyril	MEDECINE GENERALE	Médecine
BELIZNA Cristina	MEDECINE INTERNE	Médecine
BENOIT Jacqueline	PHARMACOLOGIE	Pharmacie
BERNARD Florian	ANATOMIE	Médecine
BESSAGUET Flavien	PHYSIOLOGIE PHARMACOLOGIE	Pharmacie
BLANCHET Odile	HEMATOLOGIE ; TRANSFUSION	Médecine
BOISARD Séverine	CHIMIE ANALYTIQUE	Pharmacie
BOUCHER Sophie	ORL	Médecine
BRIET Claire	ENDOCRINOLOGIE, DIABETE ET MALADIES METABOLIQUES	Médecine
BRILLAND Benoit	NEPHROLOGIE	Médecine
BRIS Céline	BIOCHIMIE ET BIOLOGIE MOLECULAIRE	Pharmacie
BRUGUIERE Antoine	PHARMACOGNOSIE	Pharmacie
CAPITAIN Olivier	CANCEROLOGIE ; RADIOTHERAPIE	Médecine
CHABRUN Floris	BIOCHIMIE ET BIOLOGIE MOLECULAIRE	Pharmacie
CHAO DE LA BARCA Juan-Manuel	BIOCHIMIE ET BIOLOGIE MOLECULAIRE	Médecine
CHOPIN Matthieu	MEDEECINE GENERALE	
CODRON Philippe	NEUROLOGIE	Médecine
DEMAS Josselin	SCIENCES DE LA READAPTATION	Médecine
DESHAYES Caroline	BACTERIOLOGIE VIROLOGIE	Pharmacie
DOUILLET Delphine	MEDECINE D'URGENCE	Médecine
FERRE Marc	BIOLOGIE MOLECULAIRE	Médecine
FORTRAT Jacques-Olivier	PHYSIOLOGIE	Médecine
GHALI Maria	MEDECINE GENERALE	Médecine
GUELFF Jessica	MEDECINE GENERALE	Médecine
HADJ MAHMOUD Dorra	IMMUNOLOGIE	Pharma
HAMEL Jean-François	BIOSTATISTIQUES, INFORMATIQUE MEDICALE	Médicale
HAMON Cédric	MEDECINE GENERALE	Médecine
HELESBEUX Jean-Jacques	CHIMIE ORGANIQUE	Pharmacie
HERIVAUX Anaïs	BIOTECHNOLOGIE	Pharmacie
HINDRE François	BIOPHYSIQUE	Médecine
JOUSSET-THULLIER Nathalie	MEDECINE LEGALE ET DROIT DE LA SANTE	Médecine
JUDALET-ILLAND Ghislaine	MEDECINE GENERALE	Médecine
KHIATI Salim	BIOCHIMIE ET BIOLOGIE MOLECULAIRE	Médecine
LEFEUVRE Caroline	BACTERIOLOGIE ; VIROLOGIE	Médecine
LEGEAY Samuel	PHARMACOCINETIQUE	Pharmacie
LEPELTIER Elise	CHIMIE GENERALE	Pharmacie
LETOURNEL Franck	BIOLOGIE CELLULAIRE	Médecine
MABILLEAU Guillaume	HISTOLOGIE, EMBRYOLOGIE ET CYTOGENETIQUE	Médecine
MALLET Sabine	CHIMIE ANALYTIQUE	Pharmacie
MAROT Agnès	PARASITOLOGIE ET MYCOLOGIE MEDICALE	Pharmacie
MESLIER Nicole	PHYSIOLOGIE	Médecine
MIOT Charline	IMMUNOLOGIE	Médecine

MOUILLIE Jean-Marc	PHILOSOPHIE	Médecine
NAIL BILLAUD Sandrine	IMMUNOLOGIE	Pharmacie
PAILHORIES Hélène	BACTERIOLOGIE-VIROLOGIE	Médecine
PAPON Xavier	ANATOMIE	Médecine
PASCO-PAPON Anne	RADIOLOGIE ET IMAGERIE MEDICALE	Médecine
PENCHAUD Anne-Laurence	SOCIOLOGIE	Médecine
PIHET Marc	PARASITOLOGIE ET MYCOLOGIE	Médecine
PIRAUX Arthur	OFFICINE	Pharmacie
POIROUX Laurent	SCIENCES INFIRMIERES	Médecine
RONY Louis	CHIRURGIE ORTHOPEDIQUE ET TRAUMATOLOGIQUE	Médecine
ROGER Emilie	PHARMACOTECHNIE	Pharmacie
SAVARY Camille	PHARMACOLOGIE-TOXICOLOGIE	Pharmacie
SCHMITT Françoise	CHIRURGIE INFANTILE	Médecine
SCHINKOWITZ Andréas	PHARMACOGNOSIE	Pharmacie
SPIESSER-ROBELET Laurence	PHARMACIE CLINIQUE ET EDUCATION THERAPEUTIQUE	Pharmacie
TEXIER-LEGENDRE Gaëlle	MEDECINE GENERALE	Médecine
VIAULT Guillaume	CHIMIE ORGANIQUE	Pharmacie

AUTRES ENSEIGNANTS

ATER		
BARAKAT Fatima	CHIMIE ANALYTIQUE	Pharmacie
ATCHADE Constantin	GALENIQUE	Pharmacie
PRCE		
AUTRET Erwan	ANGLAIS	Santé
BARBEROUSSE Michel	INFORMATIQUE	Santé
COYNE Ashley	ANGLAIS	Santé
O'SULLIVAN Kayleigh	ANGLAIS	Santé
RIVEAU Hélène	ANGLAIS	
PAST-MAST		
AUBRUCHET Hélène		
BEAUVAIS Vincent	OFFICINE	Pharmacie
BRAUD Cathie	OFFICINE	Pharmacie
CAVAILLON Pascal	PHARMACIE INDUSTRIELLE	Pharmacie
DILÉ Nathalie	OFFICINE	Pharmacie
GUILLET Anne-Françoise	PHARMACIE DEUST PREPARATEUR	Pharmacie
MOAL Frédéric	PHARMACIE CLINIQUE	Pharmacie
CHAMPAGNE Romain	MEECINE PHYSIQUE ET READAPTATION	Médecine
KAASSIS Mehdi	GASTRO-ENTEROLOGIE	Médecine
GUITTON Christophe	MEDECINE INTENSIVE-REANIMATION	Médecine
LAVIGNE Christian	MEDECINE INTERNE	Médecine

PICCOLI Giorgina	NEPHROLOGIE	Médecine
POMMIER Pascal	CANCEROLOGIE-RADIOTHERAPIE	Médecine
SAVARY Dominique	MEDECINE D'URGENCE	Médecine
PLP		
CHIKH Yamina	ECONOMIE-GESTION	Médecine

REMERCIEMENTS

Au Professeur Franck Lacœuille,

Merci de m'avoir accueilli avec bienveillance dans cette magnifique spécialité. J'ai eu la chance de rencontrer un chef de service à la fois réactif, disponible et présent aux moments clés de mon parcours.
Vous m'avez offert la liberté de façonner cet internat selon mes aspirations, ce qui a grandement renforcé l'intérêt que je porte à la recherche et à l'enseignement.
Vous avez accepté, en plus de présider ce jury, de diriger ma thèse de science autour d'un sujet que j'ai pu pleinement m'approprier et que j'ai hâte de concrétiser.
Vous avez ma plus profonde et respectueuse reconnaissance.

Au Docteur Clément Bouron,

Merci pour tes précieux conseils et ton accompagnement depuis mes premiers pas en médecine nucléaire jusqu'à aujourd'hui.
Tu m'as formé et intégré rapidement dans la prise en charge des patients, ce qui m'a permis de progresser vite mais sûrement, dans un cadre à la fois professionnel et amical.
Enfin, je te remercie d'avoir accepté de diriger cette thèse et de t'y être investi avec autant d'intérêt, de disponibilité et de rigueur.

Au Docteur Éric Gontier,

Merci pour la formation rigoureuse que tu m'as dispensée durant mon passage au Mans. Ton parcours, riche et ouvert sur de nombreuses disciplines, est une véritable source d'inspiration et a notamment renforcé mon envie de rejoindre la réserve.
Parmi tes nombreuses idées ingénieuses, du marquage d'une sonde endovasculaire (au scandium ?) à l'injection nodale *in situ*, figure cette fameuse souris non conventionnelle sur laquelle repose cette thèse.
Merci pour ce regard novateur sur la médecine nucléaire que tu m'as transmis tout au long de ce semestre.

Au Docteur Sylvie Girault,

Je vous remercie sincèrement de m'avoir proposé ce travail au moment où j'étais à la recherche d'un projet. Je vous suis également reconnaissant pour votre disponibilité tout au long de l'élaboration du protocole, ainsi que pour vos relectures attentives et toujours bienveillantes.
J'ai hâte de travailler et d'apprendre à vos côtés durant mon dernier semestre d'internat.

Au Docteur Camille Guillerminet,

Merci pour ta patience et ton enseignement. Tu m'as permis d'aborder ce sujet avec une grande liberté, tout en fixant un cadre clair qui m'a aidé à progresser dans la conception d'une étude clinique. Ta bienveillance et ta rigueur m'ont offert un environnement de travail serein et stimulant.
Merci aussi pour ta patience face à certaines difficultés que tu as su gérer avec humour et discernement.
J'aimerais beaucoup collaborer à nouveau avec toi sur de nouveaux projets.

Au Docteur Cavaro-Ménard,

Je vous remercie pour l'enseignement que vous m'avez transmis dans le cadre du Master 2 SIBM. C'est une chance de pouvoir bénéficier, à Angers, d'une formation d'une telle qualité.
Merci également pour votre soutien technique et scientifique dans la réalisation de cette thèse et d'avoir accepté de participer au jury.

À Pierre-Jean, Hervé, Laurent et Clément,

Merci pour votre enseignement patient et bienveillant. La qualité de la formation à Angers est excellente, et c'est en grande partie grâce à vous. Vous m'avez formé à l'ensemble des techniques de la spécialité, et je sais que j'ai encore beaucoup à apprendre à vos côtés.
Merci également pour les soirées passées en votre compagnie : ces moments suspendus participent pleinement à l'excellente ambiance qui règne au sein du service. Merci pour votre bonne humeur et votre générosité.

REMERCIEMENTS

À l'équipe médicale du Mans,

Merci pour votre enseignement : j'ai énormément appris à vos côtés, dans une ambiance à la fois rigoureuse et conviviale. J'ai pu y approfondir ma relation avec les patients et ma pratique des techniques échographiques.
Merci particulièrement à Éric pour son idée ingénieuse de transposer une souris gaming à la tâche d'interprétation, et pour avoir renforcé mon désir de rejoindre la réserve**.**

A l'équipe médicale de l'ICO,

Merci pour votre bonne humeur et votre convivialité. Vous avez été présent à chaque fois que c'était nécessaire, dans le recueil des données sur SubtlePET® jusqu'aux relectures.
J'ai hâte de poursuivre mon apprentissage et de travailler à vos côtés.

À mes amis de Saclay,

Jérôme, Gaël, Charles-Louis, Rachel, Lucas et Arnaud, cette formation parisienne m'a permis de faire votre connaissance et de partager avec vous des moments inoubliables. Ces semaines passées ensemble, d'une cité des Ulis jusqu'au chalet de la vallée de Chevreuse, ont été rythmées par des échanges aussi riches que délirants. Nous avons presque réussi à arriver à l'heure et éviter le premier rang, je vous en remercie. Je souhaite de tout cœur entretenir avec vous cette amitié qui m'est si chère.

À mes co-internes,

Mathieu et Bérénice, merci pour votre gentillesse. Je suis heureux de vous compter parmi mes collègues et mes amis. Mathieu, merci tout particulièrement pour le temps que tu as consacré à la participation à cette étude.
Chloé, Maya, Ludovic et Solène, grâce à vous j'ai passé un semestre à la fois enrichissant et agréable sous la bise brestoise. Je vous en remercie sincèrement et espère avoir bientôt l'occasion de partager à nouveau de bons moments à vos côtés.

Aux membres du bureau de l'ANAIMEN,

Merci pour votre sérieux et votre engagement au sein de cette association au travers de laquelle j'ai eu la chance de faire votre connaissance.
De nombreux projets nous attendent, et avec une équipe aussi dynamique et complémentaire, je suis convaincu qu'ils seront menés à bien.

REMERCIEMENTS

À mes chers parents,

Pour votre soutien indéfectible et votre amour sans faille.
Merci de m'avoir accompagné à chaque étape de ce parcours, d'avoir cru en moi lorsque le doute s'installait, et de m'avoir donné la force d'avancer.
C'est grâce à vous que cette passion pour la médecine a pu éclore, s'enraciner et grandir. Vos conseils, votre patience et votre présence constante ont été mes repères les plus précieux.
Merci pour ces innombrables allers-retours durant ma première année, pour votre écoute face à mes frustrations, et pour tous les moments réconfortants passés à vos côtés.

Si cette thèse évoque la nécessité d'adapter les interfaces utilisateurs pour tirer le meilleur parti des avancées technologiques, elle me rappelle aussi qu'un enfant, pour se construire, a besoin d'un accompagnement solide, attentif et bienveillant.
Vous m'avez offert tout cela, et bien plus encore.
Je ne vous en remercierai jamais assez.

À mon frère,

Merci pour ta présence, ton amour et ta bienveillance.
Merci tout particulièrement d'être venu régulièrement me voir à Poitiers durant les premiers moments de mon cursus : ta présence m'a été précieuse.
Suivre ton parcours, marqué par des années exigeantes mais couronnées de succès, a été pour moi une source d'inspiration et de motivation. Tes appels aux moments clés m'ont souvent permis de croire en moi et de dépasser mes limites.

J'ai trouvé en toi non seulement un frère, mais aussi un grand ami. Mon enfance a été merveilleuse grâce à toi, et nos chamailleries n'ont d'égales que la complicité indéfectible qui nous unit.
Je serai toujours à tes côtés, pour te soutenir comme tu l'as fait pour moi, et pour partager encore de nombreux moments de rires et de joie.

À ma chérie Eva,

Depuis le jour de notre rencontre, ma perception du monde a changé. Tu m'as offert un soutien quotidien sans faille et un amour infini. Sans toi, je suis convaincu que tout cela n'aurait pas été possible.
Merci pour tes conseils, ta présence et ta patience. Tu as su m'accompagner avec cette douceur et cette bienveillance qui te caractérisent.
Nous avançons ensemble vers de nouvelles perspectives, et je ne pourrais être plus heureux que de les construire à tes côtés.
Tu m'as tant apporté, et je t'en serai toujours profondément reconnaissant.

Liste des abréviations

Abréviation	Définition
3D-OSEM	3D Ordered Subsets Expectation Maximization
AI	Artificial Intelligence
BMI	Body Mass Index
CCC	Concordance Correlation Coefficient
CI	Confidence Interval
CNRS	Centre National de la Recherche Scientifique
CT	Computed Tomography
CV	Coefficient of Variation
EU	European Union
FDA	Food and Drug Administration
GLCM	Gray Level Co-occurrence Matrix
GLRLM	Gray Level Run Length Matrix
GLSZM	Gray Level Size Zone Matrix
IBSI	Image Biomarker Standardisation Initiative
ICO	Institut de Cancérologie de l'Ouest
IEC	International Electrotechnical Commission
INSERM	Institut National de la Santé et de la Recherche Médicale
IRB	Institutional Review Board
IQR	Interquartile Range
kV	Kilovolt
L1	(L1) Norm
LSO	Lutetium Oxyorthosilicate
MBq	Megabecquerel
NEMA	National Electrical Manufacturers Association
NGTDM	Neighbourhood Gray Tone Difference Matrix
OSEM	Ordered Subsets Expectation Maximization
PACS	Picture Archiving and Communication System
PCA	Principal Component Analysis
PC1	Principal Component 1
PC2	Principal Component 2
PET	Positron Emission Tomography
PET/CT	Positron Emission Tomography / Computed Tomography
PSF	Point Spread Function
PSMA	Prostate-Specific Membrane Antigen
ROI	Region of Interest
R100	Reconstruction native à 100 % du temps d'acquisition
R75	Reconstruction native à 75 % du temps d'acquisition
R50	Reconstruction native à 50 % du temps d'acquisition
S75	Reconstruction débruitée par SubtlePET® à 75 % du temps d'acquisition
S50	Reconstruction débruitée par SubtlePET® à 50 % du temps d'acquisition
SD	Standard Deviation
SSIM	Structural Similarity Index Measure
SUVbw	Standardized Uptake Value body-weight
SUVmax	Standardized Uptake Value maximum
TOF	Time Of Flight
U-Net	U-Net Convolutional Neural Network

[18F]FDG	Fluorodeoxyglucose F-18
[68Ga]PSMA	Gallium-68 Prostate-Specific Membrane Antigen
DPI	Dots Per Inch
USB	Universal Serial Bus
CHU	Centre Hospitalier Universitaire
MLEM	Maximum Likelihood Expectation Maximization
ILC	Institut Interrégional de Lutte contre le Cancer
CHM	Centre Hospitalier du Mans
LED	Light Emitting Diode
SMI	SensoMotoric Instruments
Hz	Hertz

TABLE DES MATIERES

SERMENT D'HIPPOCRATE ..... D
TABLE DES MATIERES 6
GENERAL INTRODUCTION 8

CLINICAL VALUE OF ARTIFICIAL INTELLIGENCE IN REDUCING PET IMAGE ACQUISITION TIME: ROUTINE CLINICAL VALIDATION USING QUALITATIVE, QUANTITATIVE, AND RADIOMIC ANALYSIS ON A COHORT OF 282 PATIENTS UNDERGOING [^{18}F]FDG AND [^{68}GA]PSMA PET/CT 12
ABSTRACT 13
INTRODUCTION 14
MATERIALS AND METHODS 16
1. Clinical population 16
2. Image acquisition and processing 16
3. SubtlePET® algorithm 17
4. Phantom acquisition 18
5. Image quality and quantitative analysis 18
6. Statistical analysis 19

RESULTS 21
1. Phantom analysis 21
2. Clinical analysis 22
2.1. Population 22
2.2. Qualitative analysis 24
2.3. Subgroup analysis 29
2.4. Semi-quantitative analysis 29
3. Radiomics analysis 31

DISCUSSION 35
CONCLUSION 39
BIBLIOGRAPHY 40
SUPPLEMENTARY INFORMATION 43
ONLINE RESOURCE 44

INNOVATIVE EVALUATION OF A NON-CONVENTIONAL MOUSE FOR IMAGE INTERPRETATION IN METABOLIC IMAGING: INTEGRATION OF EYE TRACKING, KINEMATIC ANALYSIS, AND QUALITATIVE FEEDBACK 46
ABSTRACT 47
INTRODUCTION 48

MATERIALS AND METHODS **50**
1. Medical study population **50**
2. Materials **50**
2.1. Computer mouse 50
2.2. Eye Tracker 52
3. Quantitative measures **52**
3.1. Study protocol 52
3.2. Eye-tracking analysis 53
3.3. Time analysis 53
3.4. Mouse Movement Analysis 53
4. Qualitative Parameters **54**
5. Statistical Analysis **54**
RESULTS **55**
1. Eye-tracking Analysis **55**
2. Time analysis **58**
3. Mouse Kinematics and Shortcuts **59**
4. Qualitative analysis **60**
DISCUSSION **62**
CONCLUSION **66**
BIBLIOGRAPHY **67**
GENERAL CONCLUSION **71**
TABLE DES MATIERES **76**

GENERAL INTRODUCTION

Since its emergence in the 1970s, PET has undergone numerous technological advances. Initially focused on the simple quantification of radioactivity, it has evolved into a multimodal analysis tool with the advent of hybrid PET/CT systems. The shift from analogue technologies to semiconductor detectors, and the replacement of filtered back-projection by iterative algorithms (MLEM, OSEM) incorporating time-of-flight and noise regularisation, have considerably strengthened its diagnostic reliability [1,2]. Now essential in the evaluation of oncological, inflammatory, infectious, and neurodegenerative diseases, PET faces a major challenge: reducing both acquisition and interpretation times. These precedent innovations have contributed, at least in part, to addressing this objective. However, the interpretative dimension, concerning image quality and manipulation, is still often relegated to the background. Furthermore, as Jacques Ellul reminded us in *La Technique ou l'enjeu du siècle* (1954): "Technology must be at the service of man, and not man at the service of technology" [3]. Faster acquisition and increased sensitivity should not come at the expense of the physician, whose interpretative task must also be facilitated to achieve the expected diagnostic improvement. It is therefore inconceivable to envisage continuous advances in acquisition and reconstruction techniques without a concomitant effort directed at user interfaces, at the risk of creating an operational barrier. Our attention is thus focused on improving these interfaces, by acting both on image quality to reduce acquisition time and on the fluidity of their manipulation to optimise interpretation. These challenges are directly related to the concept of ergonomics, initially defined as the adaptation of machines to humans (*Bonnardel, 1947* [4]), but now benefiting from a more

1. *Effect of Varying Number of OSEM Subsets on PET Lesion Detectability – 2013 A. Michael Morey and Dan J. Kadrmas*
2. *Standard OSEM vs. regularized PET image reconstruction: qualitative and quantitative comparison using phantom data - 2018 Judit Lantos*
3. *Jacques Ellul, La Technique ou l'enjeu du siècle, Paris, Armand Colin, 1954.*

complete definition. In 2000, *the International Ergonomics Association* [5] redefined ergonomics as the science concerned with the fundamental understanding of interactions between humans and other components of a system, as well as the associated profession that applies theoretical principles, data, and methods to optimise human well-being and overall system performance. When transposed to the medical field, this definition emphasises the need to evaluate any new imaging tool before its adoption, to guarantee the maintenance of optimal diagnostic quality and smooth data handling, without complicating the interpretative task. Applied to the medical field, this definition underlines the need to evaluate any new image enhancement tool prior to its adoption, to guarantee optimal diagnostic quality and seamless data handling, without complicating the interpretative task. Building on this new definition and starting from the theoretical framework, we hypothesise that denoising images acquired with reduced acquisition time can preserve sufficient diagnostic quality, improve session efficiency, shorten patient waiting times, and ensure the consistency of radiomic features. Likewise, the use of a mouse specifically designed for intensive use, offering both accessibility and sensitivity, could optimise the interpretative task and reduce its duration. Nevertheless, these innovations raise several concerns, particularly regarding the risk of alterations in quantitative data, the opacity of artificial intelligence algorithms often described as "black boxes", and the uncertainties surrounding the generalisability of models developed from non-representative populations [6]. Moreover, the devices used daily by nuclear physicians such as keyboards, mice and reading consoles could directly influence visual strategies, cognitive load and ultimately diagnostic performance. Their evolution has paralleled that of consumer computing, with little consideration given to the specific requirements

4. Bonnardel, R. L'Adaptation de l'homme à son métier : étude de psychologie sociale et industrielle. Presses Universitaires de France, 1943
5. International Ergonomics Association. What is Ergonomics (or human factors) – 2000
6. Yavar Bathaee, The Artificial Intelligence Black Box and the Failure of Intent and Causation, Harvard Journal of Law & Technology, 2018.

of medicine. Yet, an unsuitable interface may slow down reading, hinder reasoning or induce errors, whereas an ergonomic and customisable interface inspired by the gaming field could instead enhance fluidity and precision. Regardless of the underlying assumptions, integration into clinical practice can only be envisaged through rigorous evaluation. The very term ergonomics, derived from the ancient Greek words *"ergon"* meaning work and *"nomos"* meaning law, resonates here with particular relevance to the ethical and professional principles of our discipline.

Regarding the data and methods envisaged, this work will rely on innovative approaches designed to enable the extraction of objective quantitative data suitable for robust comparative analyses. Radiomic analysis of denoised images will provide an objective assessment of the impact of these technologies on the consistency of the extracted data. In parallel, the study of visual interpretation strategies using eye tracking, with and without the use of a non-conventional pointing device, will offer new insights into the way ergonomics influences diagnostic performance.

Finally, we will assess the concept of well-being through a subjective qualitative analysis conducted among physicians. This will encompass the cognitive dimension by examining mental workload and interaction with software, the organisational dimension through the integration of tools into the workflow, and the diagnostic dimension in terms of errors and interpretation time. The aim will be to evaluate nuclear physicians' acceptance of these innovations, their impact on clinical practice, and the confidence placed in these devices.

This thesis is situated within the current and future context in which artificial intelligence and interface ergonomics are becoming major areas of

improvement. Its ambition is twofold: to strengthen the quality, speed, and reliability of interpretation, while at the same time improving clinicians' working conditions. By providing concrete and applicable data, this work seeks to demonstrate how technological innovation, when conceived from an ergonomic perspective, can be seamlessly integrated into clinical practice and support more appropriate patient care.

CLINICAL VALUE OF ARTIFICIAL INTELLIGENCE IN REDUCING PET IMAGE ACQUISITION TIME: ROUTINE CLINICAL VALIDATION USING QUALITATIVE, QUANTITATIVE, AND RADIOMIC ANALYSIS ON A COHORT OF 282 PATIENTS UNDERGOING [^{18}F]FDG AND [^{68}GA]PSMA PET/CT

A Dambrain[1], PA Dufour[2], M Lacombe[2], F Lacoeuille[3], O Morel[2], A Testard[2], C Bouron[1], S Girault[2], C Guillerminet[4]

1. MD, University Hospital of Angers, France
2. MD, Department of Nuclear Medicine, Institut de Cancérologie de l'Ouest (ICO), Paul Papin Center, Angers, France
3. PharmD, PhD, Radiopharmacist, CRCI^{2}NA- Inserm UMR1307/CNRS UMR 6075, Université d'Angers, CHU d'Angers, France
4. Medical physicist, Department of Medical Physics, Institut de Cancérologie de l'Ouest (ICO), Paul Papin Center, Angers, France

ABSTRACT

ABSTRACT

Purpose We evaluated the impact of AI-based denoising on PET exams acquired with reduced acquisition times using [^{18}F]FDG and [^{68}Ga]PSMA.

Methods We reconstructed three sets of images: 100% acquisition time (R100), 75% (R75), and 50% (R50), with their respective denoised versions using SubtlePET® (S75 and S50). On a NEMA phantom, we analysed six contrasts (12:1–2:1) using [^{18}F]FDG, assessing contrast, background noise, and radiomic features. In a prospective cohort of 282 patients injected with [^{18}F]FDG and [^{68}Ga]PSMA, five nuclear physicians performed a qualitative evaluation of image quality and confidence in the presence of hypermetabolism in 634 lesions. 162 radiomic features from 105 lesions were compared between the original and denoised reconstructions.

Results The phantom study showed no difference in sphere contrast, a reduction in background noise variability, and excellent preservation of radiomic features. In the clinical population, S75 images showed improvements across all criteria evaluated, except for diagnostic confidence, which remained higher with R75 ($p = 0.555$ when compared to R100) for [^{18}F]FDG. For [^{68}Ga]PSMA, only S50 images showed a significant degradation in liver image quality. A decrease in SUVmax was observed in denoised images (-7.73% for [^{18}F]FDG; -11.46% for [^{68}Ga]PSMA, $p < 0.0001$). The radiomic analysis demonstrated excellent correlation, with a concordance correlation coefficient (CCC) > 0.8 for 90% of radiomic features.

Conclusions SubtlePET® improves image quality of PET acquisitions performed with reduced acquisition times using [^{18}F]FDG and [^{68}Ga]PSMA. However, clinician confidence remains limited. For the first time, we demonstrate the preservation of radiomic features despite reduced acquisition times.

Keywords: AI, artificial intelligence, denoising, radiomics, PET, SubtlePET®

Introduction

Over the past decade, the number of combined positron emission tomography and computed tomography (PET/CT) scans has tripled in France (1). The increase in examinations and the need to maintain acceptable waiting times for scheduling have led to efforts to reduce acquisition time, offering medical, economic, and patient comfort benefits (2). Historically, the main solutions currently available have relied on transitioning from filtered back-projection reconstruction to iterative reconstruction using the ordered subset expectation maximisation (OSEM) algorithm, followed by the development of semiconductor technology (3) and, more recently, software such as Q.Clear® (4). However, these reconstruction methods have limitations, particularly regarding alterations in qualitative and quantitative imaging characteristics (5). As image quality is directly proportional to the number of coincidences detected, reducing either the amount of radiotracer or the acquisition time leads to the same consequence: an increase in image noise. This degradation negatively impacts diagnostic performance, especially in areas with low metabolic contrast (6), and detecting small structures is affected by the partial volume effect.

SubtlePET® is an American software solution approved by the FDA and the European Union since 2018, making it the first artificial intelligence (AI) software entirely dedicated to nuclear medicine. Developed using a U-Net convolutional neural network, it makes it possible to reduce both acquisition time and required dose of radiotracer by denoising images acquired through standard protocols (7). However, its use presents certain limitations, such as the frequent alteration of semi-quantitative values, particularly the standardised uptake value (SUV), which can vary by up to 15% (2,6,8). Nevertheless, these changes are not systematically observed and do not impact diagnostic quality or clinician confidence in interpreted scans (9).

To date, only a few studies in the literature have analysed the processing of standardised phantom images, demonstrating improved image quality with reduced acquisition time compared to non-denoised images (10,11). Additionally, only one publication has assessed the impact of AI-based denoising on extracted radiomic data, without modifying acquisition time (12). While this study is promising and shows strong correlation, further research is needed to validate these findings, particularly in clinical settings and with reduced acquisition times.

In this prospective study, we evaluate the denoising impact of SubtlePET® on phantom and clinical images, within a single cohort including both [^{18}F]FDG (fluoro-2-désoxy-D-glucose) and [^{68}Ga]PSMA (prostate-specific membrane antigen) PET scans. For the first time, we also explore the correlation of radiomic features obtained with reduced acquisition time.

MATERIALS AND METHODS

1. Clinical population

We prospectively included 282 patients who underwent a PET/CT examination between March and April 2024 at the Institut de Cancérologie de l'Ouest (ICO), using one of two radiotracers: [^{18}F]FDG or [^{68}Ga]PSMA. No specific selection was made regarding the indication or other condition. However, as the study was conducted in a cancer treatment centre, most indications were oncological in nature.

The study protocol was submitted to the local institutional review board (IRB) in February 2024 (reference no. 2025143). All patients provided informed consent for the use of their data.

2. Image acquisition and processing

For [^{18}F]FDG examinations, the standard acquisition protocol included a 6-hour fasting period, administration of 3 MBq/kg, a 60-minute uptake time, and a scan duration of 60 seconds per step. For patients with a body mass index (BMI) > 35, the acquisition time was increased to 90 seconds per step. Patients receiving a [^{68}Ga]PSMA injection were administered a standard dose of 150 MBq, with a 60-minute uptake time before image acquisition lasting 90 seconds per bed position, and no fasting was required. All images were acquired in accordance with the recommendations of the European Association of Nuclear Medicine, using a Philips VEREOS PET scanner. This digital system is equipped with LSO (lutetium oxyorthosilicate) crystals and silicon photomultipliers, incorporating time-of-flight technology. Image reconstruction was performed using the 3D-OSEM algorithm, with 2 iterations and 4 subsets, with point spread function (PSF) correction. The matrix size was 288 x 288, with a voxel size of 2 x 2 x 2 mm. The CT scan parameters were 100–140 kV; the acquisition was performed with 64 × 0.625 mm collimation and reconstructed at 1.5 mm, using mAs modulation including both 3D and Z-axis modulation, with an iterative reconstruction level of iDose^4 set to 5. The field of view

covered at least the skull base to the upper thighs and could be extended to a whole-body acquisition if needed.

For each patient, two additional image series were reconstructed from list-mode data by artificially reducing the count statistics to simulate acquisitions at 75% and 50% of the standard acquisition time. These series were post-processed either using the 3D-OSEM algorithm alone (R100, R75) or with both the 3D-OSEM algorithm and the SubtlePET® noise reduction algorithm (S75, S50).

3. SubtlePET® algorithm

The SubtlePET® software version 2.0.2. was developed by Subtle Medical (CA, USA) and has been approved by both the FDA and the European Union since 2018. Its primary goal is to reduce PET image acquisition time without compromising quality or clinical information. It is based on a U-net convolutional neural network algorithm trained on a dataset acquired under both standard and reduced acquisition conditions, using data from 13 different PET scanner models and including patient cases ranging in age from 2 to 86 years. Eight radiotracers were used to train the model. The average injected dose was 6 MBq/kg for [^{18}F]FDG, with an average acquisition time of 2-3 minutes per bed position. The software processes structural data in 2.5D and has been trained on various types of PET/CT images and clinical indications. The neural network partly relies on the L1 norm and the structural similarity index measure. After automated anonymisation, the locally reconstructed images are sent to the SubtlePET® server for remote post-processing, then returned and integrated into the picture archiving and communication system. This software is commercially available, and the license was funded by the ICO.

4. Phantom acquisition

We used a standard NEMA IEC body phantom (background volume: 9700 mL) containing six spheres with inner diameters of 10, 13, 17, 22, 28, and 37 mm. A solution of [^{18}F]FDG was diluted in 1000 mL of water to achieve target-to-background contrast ratios of 12:1, 10:1, 8:1, 6:1, 4:1, and 2:1 (C1 to C6). The phantom was centred in the PET field of view, and the images were acquired in the usual manner. In accordance with NEMA NU 2-2018 standards, we calculated the percentage contrast for each sphere j (QH,j) and the percentage background variability (Nj) by manually defining regions of interest (ROI) on the spheres of the phantom and on the adjacent background, for each contrast based on CT images.

$$QH,j = \frac{\frac{C_{H,j}}{C_{B,j}} - 1}{\frac{a_H}{a_B} - 1} \times 100\% \qquad N_j = \frac{SD_j}{C_{B,j}} \times 100\%$$

We selected four robust radiomic features minimally influenced by sphere size variations (13–15): SUVmax (IBSI: 84IY), Skewness (IBSI: KE2A), Kurtosis (K) (IBSI: IPH6), and intensity-histogram_AreaUnderCurveCIVH (IBSI: No).

5. Image quality and quantitative analysis

Qualitative image analysis was performed by a nuclear physician different from the one who made the initial diagnosis, in order to avoid bias in the evaluation of the noise-reduced reconstructions. Five nuclear physicians, each with more than five years' experience, conducted this qualitative assessment. A dedicated study workflow on Syngo.via® VB60A was established, making possible simultaneous visualisation of the five image reconstructions and facilitating comparative analysis.

An evaluation grid specific to each patient, including both qualitative and quantitative analysis of the examination, had to be completed by the nuclear physicians. For this purpose, they selected the most diagnostically relevant lesions for each report. A ROI was drawn on each

selected lesion to extract the SUVmax, which was then recorded in the grid, along with the nature of the lesion (nodal, visceral, hepatic, or osseous) and the location of the primary lesion. The qualitative evaluation criteria were collected using a dedicated grid for each examination and rated on a 5-point Likert scale. The criteria included overall examination quality, the quality of the signal from the hepatic parenchyma, and confidence in the presence of true hypermetabolism for each lesion. A global assessment was then performed, incorporating examination quality, global noise, hepatic heterogeneity, interpretation speed, and how confident the nuclear physicians were in their diagnosis if they had been tasked with interpreting these images. Each nuclear physician could note any comments that they considered relevant.

For the radiomics analysis, 636 lesions were initially identified. To ensure homogeneity, only lesions from patients with breast, lung or prostate cancer were included, resulting in 336 lesions. Thirteen very small lesions were excluded because they could not be segmented by the SubtlePET® software. From the remaining set, 105 lesions were randomly selected, without specific criteria, and segmented using a 40% 3D isocontour of the maximal pixel value with a semi-automatic tool on Syngo.via® VB60A by an independent operator. The segmentations were then transferred to LifeX 7.6.9 (16) to extract 162 radiomic features. The images had a native isotropic resolution of 2×2×2 mm, making an interpolation step unnecessary. As there is no consensus on intensity discretisation, a fixed bin number of 35 was applied, corresponding to the maximum SUVmax observed across the dataset.

6. Statistical analysis

All statistical analyses and figure generations were conducted using the R software (version 4.4.2) and Python code (version 3.12). Categorical variables were represented by counts and percentages. Continuous variables were described by their mean, median, and interquartile range (IQR). Size effects for semi-quantitative variables (SUVmax) were assessed using

Cohen's d, and the coefficient of variation (CV) was calculated across reconstruction types to evaluate measurement consistency. Ordinal variables (based on a 5-point Likert scale) were compared using Friedman's two-way analysis of variance by rank followed by Conover's post-hoc test. To assess potential observer bias from different post-processing, a principal component analysis (PCA) was conducted after having standardised and linearly approximated the ordinal variables to make PCA possible. The radiomic features were analysed with the aim of identifying the existence of a correlation between the standard reconstruction (R100) and the other reconstruction types. A concordance correlation coefficient (CCC) was then calculated between the different R100 reconstructions and other images with time reduction (R75, R50) and denoising (S75 and S50). All p-values were obtained using a two-sided test, with a significance threshold set at 5%, chosen for its widespread use.

RESULTS

1. Phantom analysis

To explore the impact of acquisition time and denoising on image quality in a controlled setting, standardised phantom datasets were analysed. The initial analyses focused on detectability metrics, encompassing both contrast and background noise, to assess the system's ability to distinguish relevant signals from background activity. The reduction in acquisition time resulted in a marked increase in noise, which was further accentuated by the decrease in contrast. Denoising helped the entire phantom (spheres and background) recover a more homogeneous appearance, but did not make it possible to recover the signal from the smallest spheres (arrow), which was lost in noise in the 2:1 contrast condition (10 mm inner diameter spheres in R75 and 10 and 13 mm inner diameter spheres in R50), as illustrated in Figure 1.

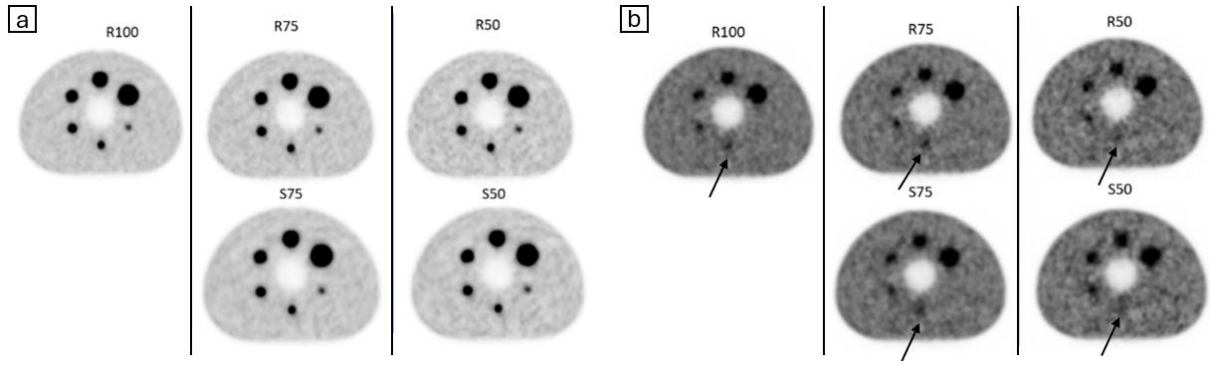


Fig. 1 Acquisition of a NEMA phantom with contrast 8:1 (a) and contrast 2:1 (b), according to acquisition time and the use of SubtlePET®. The arrow highlights the evolution in the signal of 13 inner diameter spheres in contrast 2:1.

The variability in background noise for each phantom contrast and each reconstruction method is illustrated in Figure 2. Using SubtlePET® software showed a trend toward improvement, with a reduction in background variability for images acquired with 75% and 50% of the normal acquisition time processed by AI, compared to standard reconstructions. It should be noted that an increase in background noise variability was, as expected, correlated with the reduction

in acquisition time. Sphere-to-background contrast decreased with smaller spheres and higher background activity, regardless of acquisition time or AI-based denoising (Online Resource 1).

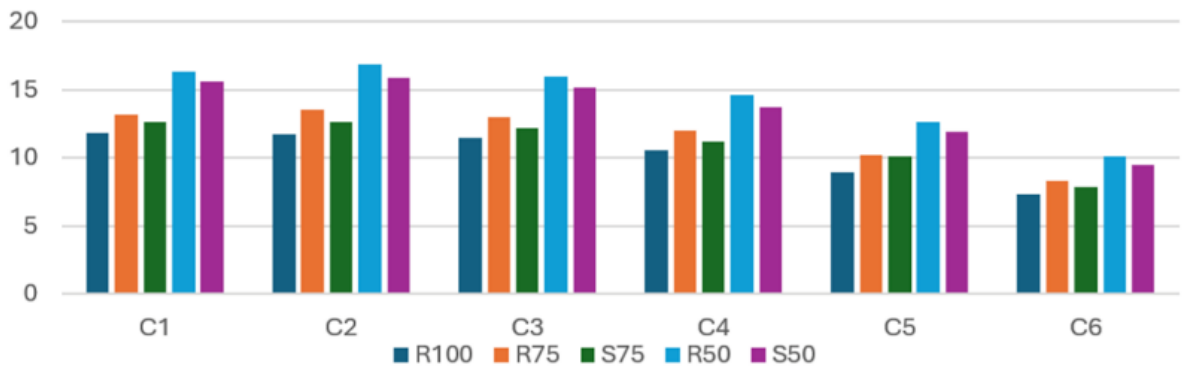


Fig. 2 Background noise variability (% on the y-axis) according to acquisition time (R100, R75, R50) and denoising with SubtlePET® (S75, S50) for each of the 6 phantom contrasts (C1 to C6).

The second part of the analysis focused on radiomic features extracted from the phantoms, making it possible to assess intensity patterns, noise distribution, and overall structural consistency quantitatively across reconstructions. These features (SUVmax, Kurtosis, Skewness, intensity_histogramAreaUnderCurveCIVH) showed excellent correlation across all reconstructions (CCC > 0.9) with no significant differences from the native reconstruction according to the Friedman test. This confirms both the reliability and stability of radiomic feature extraction in this phantom setting.

2. Clinical analysis

2.1. Population

To validate these findings in real-world conditions, a clinical analysis was conducted on a cohort of routine PET/CT examinations, excluding R50 reconstructions which appeared too degraded in the phantom analysis. From March to April 2024, 282 patients were included, with a majority of women and the [^{18}F]FDG radiotracer. Three patients were excluded for undergoing a PET

scan other than [^{68}Ga]PSMA or [^{18}F]FDG, and seven due to incomplete evaluation grid data (Figure 3).

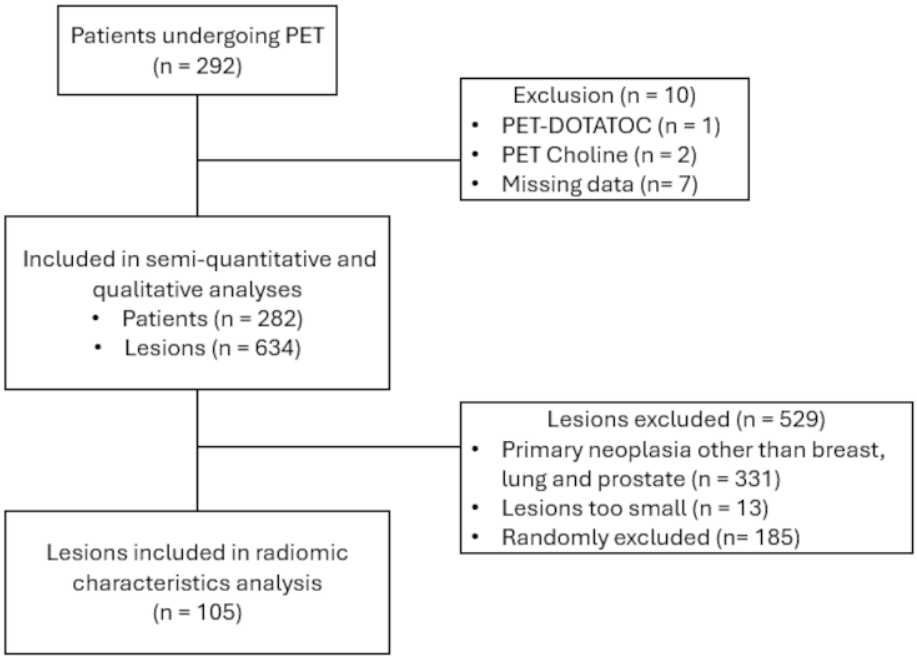


Fig. 3 Flow chart of patient selection and exclusion criteria for qualitative, semi-quantitative, and radiomic analyses.

The median age was 67 years old, and median weight was 70 kg. The main characteristics of the 282 patients included in this study are shown in Table I. Indications were mostly oncological, with a predominance of primary breast neoplasms, followed by lung neoplasms explored with [^{18}F]FDG, and prostate cancers explored with [^{68}Ga]PSMA. A total of 634 lesions were analysed, primarily categorised as nodal, visceral, and bone lesions.

Table I Baseline characteristics of the study population (*: only for [^{18}F]FDG).

Patients n = 282		
Age (median, IQR)	**67**	57-75
Male (number, %)	**101**	36.82
Female (number, %)	**181**	64.18
BMI > 35 (%)	**13**	4.6
Weight kg, (median, IQR)	**70**	61-81
BMI (median, IQR)	**25**	22.5-29.3
Blood glucose* g/L, (median, IQR)	**0.98**	0.9-1.1
Radiotracer		
[^{18}F]FDG (number, %)	**256**	90.78
[^{68}Ga]PSMA (number, %)	**26**	9.22
Primary tumours		
Breast (number, %)	**104**	36.5
Lung (number, %)	**41**	14.4
Prostate (number, %)	**27**	9.5
Digestive (number, %)	**29**	10.1
Other (number, %)	**84**	29.5
Lesion location (n = 634)		
Nodal (number, %)	**199**	31.4
Visceral (number, %)	**199**	31.4
Bone (number, %)	**131**	20.6
Others (breast, subcutaneous, muscular, head and neck) (number, %)	**105**	16.6

2.2. Qualitative analysis

To evaluate the impact of reconstruction protocols on inter-observer variability and radiotracer-related bias, a PCA was performed based on qualitative image assessment scores and is shown in Figure 4 and Table II in the appendix. The components identified reflected, on the one hand, the technical quality of the image (PC1: whole-body quality, hepatic parenchyma quality, global noise, and hepatic noise) and, on the other, the clinical efficiency of interpretation (PC2: reading speed and diagnostic confidence). The R100 protocol showed the lowest inter-observer variability, with mean distances of 1.22 on PC1 and 0.67 on PC2, without significant variability between physicians ($p = 0.52$) or between radiotracers ($p = 0.32$). In comparison, R75 showed greater dispersion in technical features (PC1: 1.38), with significant inter-observer variability ($p = 0.008$) and radiotracer-related bias ($p = 0.009$), while clinical evaluation remained close to R100 (PC2: 0.61). S75 demonstrated a marked reduction in inter-observer distances for technical features (PC1: 0.69), with clinical distances comparable to those of R75 and R100

(PC2: 0.59) and showed reduced radiotracer-related bias (p = 0.093), despite persistent inter-observer variability (p = 0.006).

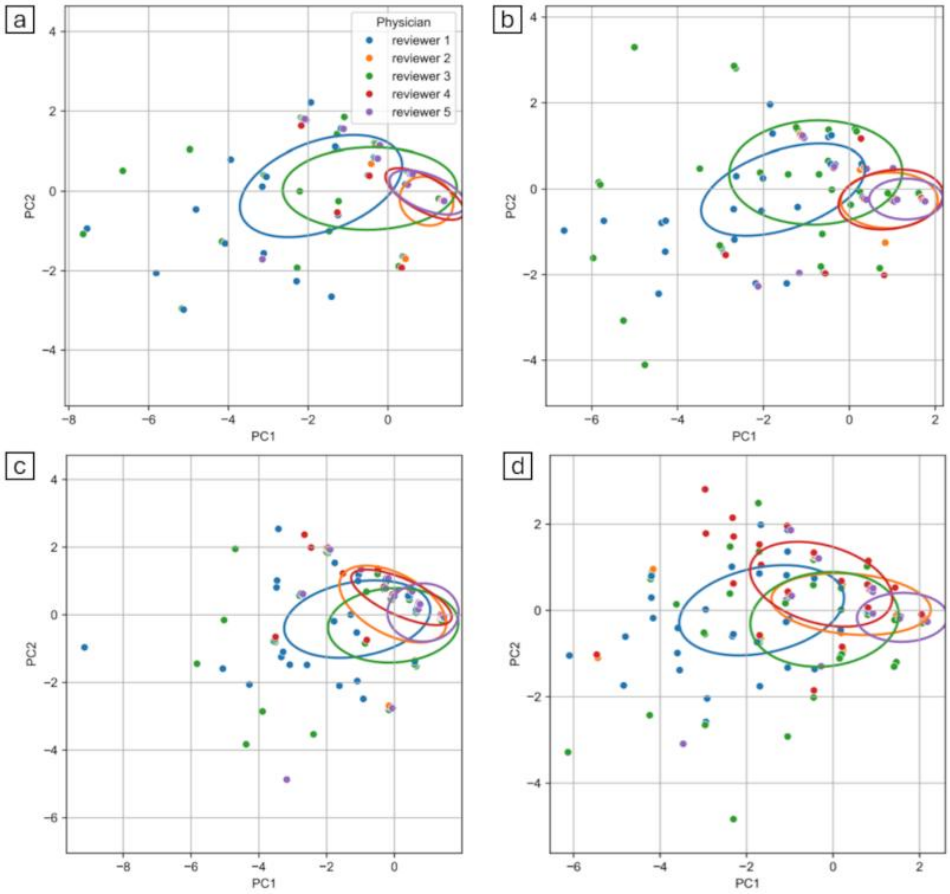


Fig. 4 PCA of qualitative scores per reconstruction protocol: (a) R100 (b) R75 (c) S75 (d) S50. Each point represents an individual evaluation with each colour indicating a different reviewer. Ellipses indicate inter-observer variability (95% confidence interval).

To complement the multivariate analysis of inter-observer variability, individual qualitative scores were examined in detail for each reconstruction protocol. Figures 5 and 6 present the scores assigned to general image quality criteria for [^{18}F]FDG and [^{68}Ga]PSMA examinations, while Tables III and IV summarise the corresponding statistical comparisons between the different reconstruction methods. The alluvial plots show that most criteria were rated 4 or 5 across all reconstructions for both radiotracers.

In the [^{18}F]FDG subgroup, no significant difference was observed between R100 and S75 (p > 0.05) in terms of overall image quality, liver signal, global hepatic noise, or interpretation

speed. However, R75 and S50 were associated with a noticeable increase in lower scores (2 or 3), particularly regarding liver image quality, hepatic noise, and diagnostic confidence. These degradations were statistically significant ($p < 0.0001$). Moreover, diagnostic confidence was significantly reduced in denoised images (S75 and S50) compared to non-post-processed reconstructions (R100 and R75), with p-values < 0.0001 (see alluvial plot and Table III).

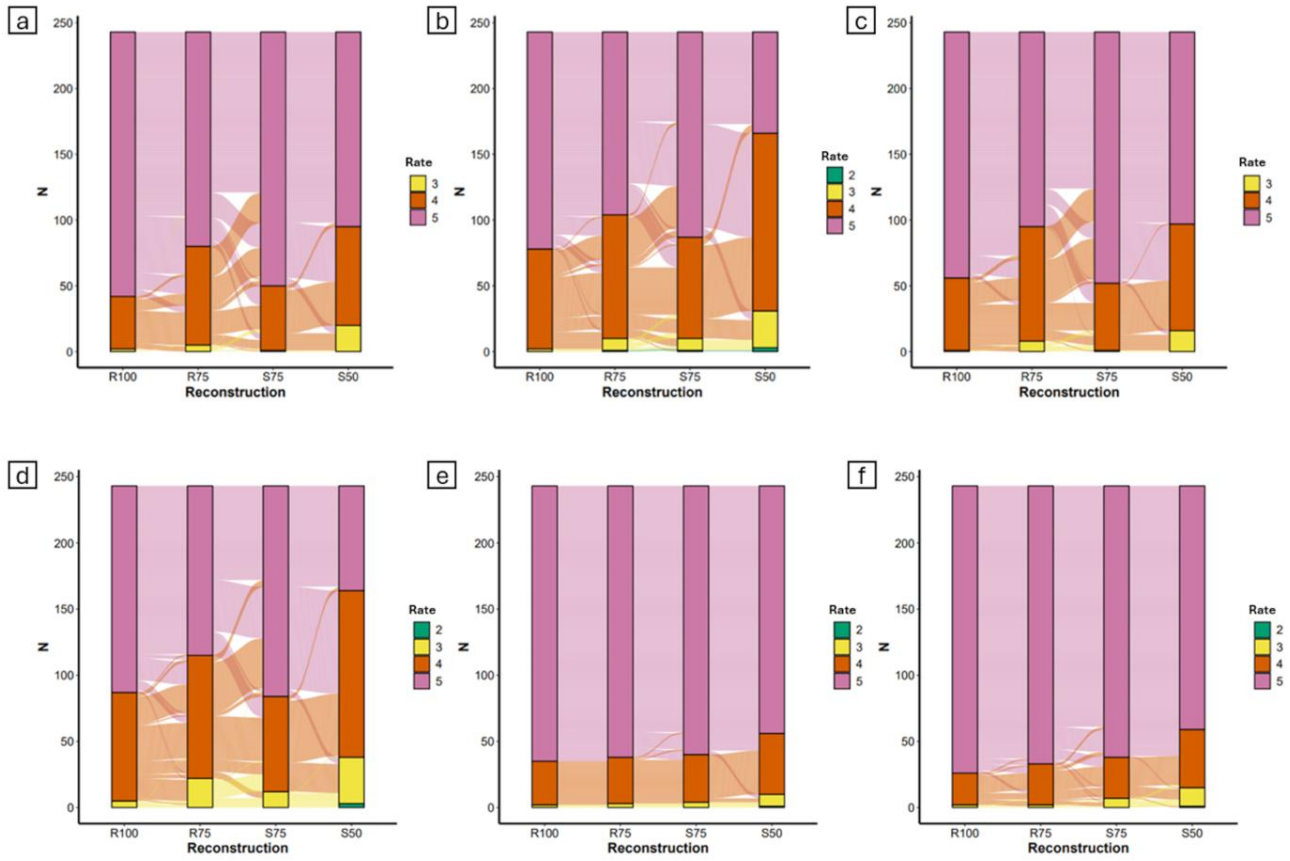


Fig. 5 Alluvial charts illustrating the distribution of scores (from 2 to 5) assigned to various image characteristics according to reconstruction methods (R100, R75, S75, S50) for the [^{18}F]FDG radiotracer. The coloured flows show how these scores shift between reconstruction methods. The criteria evaluated include: whole-body image quality (a), liver image quality (b), global noise (c), liver heterogeneity (d), interpretation speed (e), and diagnostic confidence (f).

Table III Comparison of different reconstruction methods for the global assessment criteria of the examination, with or without denoising, for the [^{18}F]FDG radiotracer (ns: not significant; p: p-value; *: p-value < 0.05; **: p-value < 0.0001).

	Whole body quality		Liver quality		Global noise		Liver heterogeneity		Interpretation speed		Diagnostic confidence	
Comparison	**p**	**Trend**	**p**	**Trend**	**p**	**Trend**	**p**	**Trend**	**p**	**Trend**	**p**	**Trend**
R100 vs R75	**	R100 > R75	**	R100 > R75	**	R100 > R75	**	R100 > R75	ns	R100 = R75	ns	R100 = R75
R100 vs S75	ns	R100 = S75	ns	R100 = S75	ns	R100 = S75	ns	R100 = S75	ns	R100 = S75	*	R100 > S75
R100 vs S50	**	R100 > S50	**	R100 > S50	**	R100 > S50	**	R100 > S50	**	R100 > S50	**	R100 > S50
R75 vs S75	**	R75 < S75	ns	R75 = S75	**	R75 < S75	**	R75 < S75	ns	R75 = S75	ns	R75 = S75
R75 vs S50	*	R75 > S50	**	R75 > S50	ns	R75 = S50	**	R75 > S50	**	R75 > S50	**	R75 > S50
S75 vs S50	**	S75 > S50	**	S75 > S50	**	S75 > S50	**	S75 > S50	**	S75 > S50	**	S75 > S50

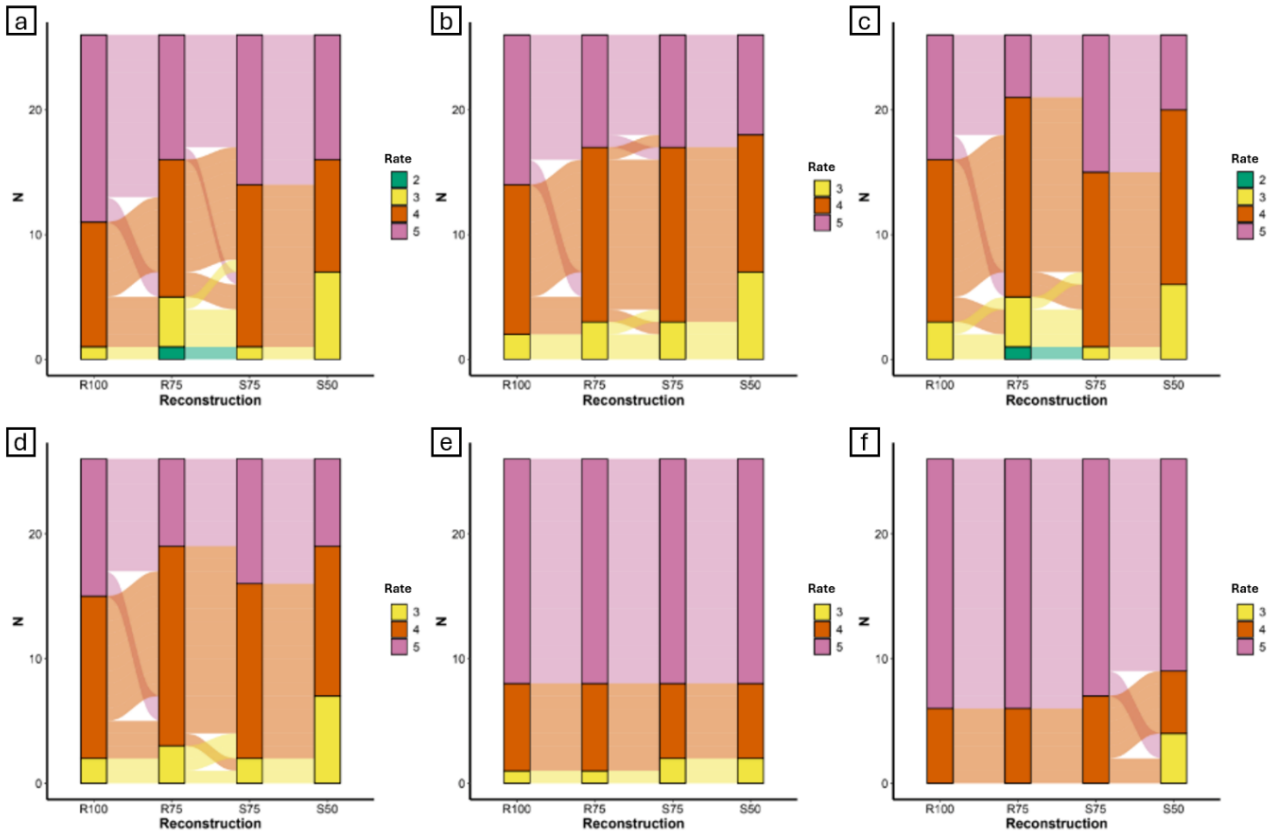


Fig. 6 Alluvial charts illustrating the distribution of scores (from 2 to 5) assigned to various image characteristics according to reconstruction methods (R100, R75, S75, S50) for the [^{68}Ga]PSMA radiotracer. The coloured flows show how these scores shift between reconstruction methods. The criteria evaluated include: whole-body image quality (a), liver image quality (b), global noise (c), liver heterogeneity (d), interpretation speed (e), and diagnostic confidence (f).

In contrast to the [^{18}F]FDG subgroup, images acquired with [^{68}Ga]PSMA showed no significant differences across reconstruction protocols for most qualitative criteria. However, hepatic parenchyma quality and global noise were significantly degraded in noise-reduced S50 images, as shown in Figure 6 and detailed in Table IV.

Table IV Comparison of different reconstruction methods for the global assessment criteria of the examination, with or without denoising, for the [^{68}Ga]PSMA radiotracer (ns: not significant; p: p-value; *: p-value < 0.05; **: p-value < 0.0001).

	Whole body quality		Liver quality		Global noise		Liver heterogeneity		Interpretation speed		Diagnostic confidence	
Comparison	**p**	**Trend**	**p.**	**Trend**	**p**	**Trend**	**p**	**Trend**	**p**	**Trend**	**p**	**Trend**
R100 vs R75	ns	R100 = R75	ns	R100 = R75	ns	R100 = R75	ns	R100 = R75	ns	R100 = R75	ns	R100 = R75
R100 vs S75	ns	R100 = S75	ns	R100 = S75	ns	R100 = S75	ns	R100 = S75	ns	R100 = S75	ns	R100 = S75
R100 vs S50	ns	R100 = S50	*	R100 > S50	ns	R100 = S50	**	R100 > S50	ns	R100 = S50	ns	R100 = S50
R75 vs S75	ns	R75 = S75	ns	R75 = S75	ns	R75 = S75	ns	R75 = S75	ns	R75 = S75	ns	R75 = S75
R75 vs S50	ns	R75 = S50	*	R75 > S50	ns	R75 = S50	*	R75 > S50	ns	R75 = S50	ns	R75 = S50
S75 vs S50	ns	S75 = S50	*	S75 > S50	ns	S75 = S50	*	S75 > S50	ns	S75 = S50	ns	S75 = S50

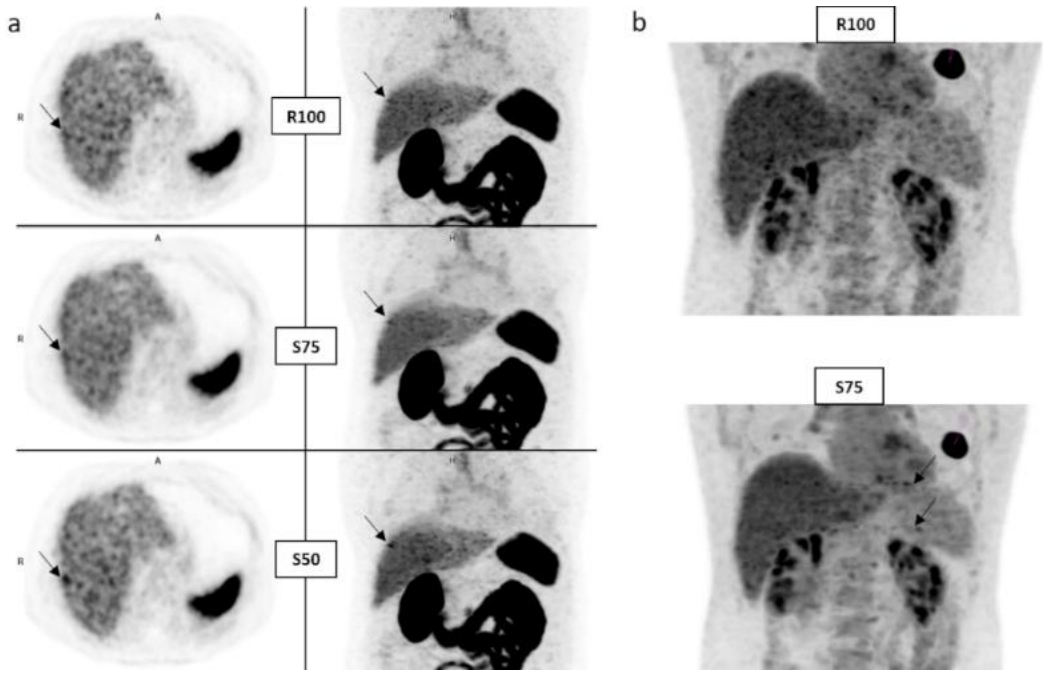


Fig. 7 Acquisition of the hepatic parenchyma from the same exam showing focal hypermetabolism on the S50 image (a). Appearance of band artefacts at the overlap margin on the S75 reconstruction (b).

To further explore these perceptions, physicians were also invited to comment on specific image alterations they attributed to shortened acquisition time or denoising. During image review, they reported a loss of spatial resolution in hepatic metabolism and, on three occasions, the appearance of heterogeneity on denoised images that could have been misinterpreted as a lesion. The presence of hypersignal bands related to overlap margin artifacts (Figure 7) was also noted.

2.3. Subgroup analysis

In the subgroup analysis evaluating diagnostic confidence in the presence of significant hypermetabolism (Table V) according to lesion type, no statistically significant difference was observed between native images and those acquired with 75% of the acquisition time without denoising, regardless of tissue type. However, the denoising led to a decrease in confidence scores for nodal and visceral lesions when images were acquired with 75% of the acquisition time. This impact was even more pronounced when the acquisition time was reduced to 50%, with a decline in confidence about significant hypermetabolism observed across all tissue categories. In the subgroup of BMI > 35 patients (n = 18), no significant difference was found, regardless of the acquisition duration or the presence of noise reduction.

Table V Confidence in the presence of significant hypermetabolism in [^{18}F]FDG PET/CT, per lesion type, according to acquisition time reduction and denoising (ns: not significant; p: p-value; *: p-value < 0.05; **: p-value < 0.0001).

	Lymphatic node		Visceral tissue		Bone		Liver	
Comparison	**p**	**Trend**	**p**	**Trend**	**p**	**Trend**	**p**	**Trend**
R100 - R75	ns	R100 = R75	ns	R100 = R75	ns	R100 = R75	ns	R100 = R75
R100 - S75	*	R100 > S75	*	R100 > S75	ns	R100 = S75	ns	R100 = S75
R100 - S50	ns	R100 = S50	*	R100 > S50	**	R100 > S50	ns	R100 = S50

2.4. Semi-quantitative analysis

In addition to visual and perceptual evaluation, the potential impact of reconstruction and denoising on quantitative metrics was assessed through SUVmax comparisons, considering

acquisition time, post-processing, radiotracer type ([^{18}F]FDG and [^{68}Ga]PSMA), and tissue subtype. Regarding the semi-quantitative analysis of SUVmax for [^{18}F]FDG (Table VI), a significant decrease in values was observed between the native reconstruction and the noise-reduced reconstructions, with a median difference for S75 and S50 of -0.3 (-7.73%, $p < 0.0001$) and -0.24 (-6.29%, $p < 0.0001$), respectively.

Table VI Comparison of SUVmax values (median, mean, minimum, and maximum) for [^{18}F]FDG images depending on acquisition time and SubtlePET® denoising, relative to R100 ; IQR : Interquartile range ; 95% CI : 95% confidence interval ; ΔSUVmax (%): mean individual % change vs R100.

[^{18}F]FDG (n = 550)				
Reconstruction	**R100**	**R75**	**S75**	**S50**
Median (IQR)	3.84 (2.73; 6.24)	3.88 (2.79; 6.20)	3.48 (2.45; 5.68)	3.51 (2.57; 5.81)
Mean [min–max]	5.29 [0.6; 37.71]	5.35 [0.8; 36.49]	4.98 [0.7; 35.6]	5.02 [0.65; 35.72]
Comparison to R100				
Mean ΔSUVmax (%)		1.92	-7.73	-6.29
Median difference (95% CI)		0.06 (0.03; 0.08)	-0.3 (-0.32; -0.27)	0.24 (0.2; 0.3)
p-value		< 0.0001	< 0.0001	< 0.0001
Deviation by tissue (% vs R100)				
Bone		4.74	4.78	4.40
Liver		5.07	5.19	4.75
Lymphatic nodes		4.66	4.70	4.33
Other visceral tissues		5.75	5.83	5.44

Table VII Comparison of SUVmax values (median, mean, minimum, and maximum) for [^{68}Ga]PSMA images depending on acquisition time and SubtlePET® denoising, relative to R100 ; IQR : Interquartile range ; 95% CI : 95% confidence interval ; ΔSUVmax (%): mean individual % change vs R100.

[^{68}Ga]PSMA (n= 76)				
Reconstruction	**R100**	**R75**	**S75**	**S50**
Median (IQR)	5.22 (3.26 ; 12.19)	5.37 (3.32 ; 12.59)	4.77 (2.84 ; 11.34)	4.76 (2.73 ; 11.20)
Mean [min–max]	9.72 [0.75 ; 61.93]	9.76 [0.82 ; 59.72]	8.87 [0.66 ; 57.55]	8.91 [0.59 ; 57.09]
Comparison to R100				
Mean ΔSUVmax (%)		2.55	-11.46	-9.79
Median difference (95% CI)		0.09 (-0.07 ; 0.2)	-0.69 (-0.91 ; -0.33)	-0.44 (-0.9 ; -0.3)
p-value		ns	< 0.0001	< 0.0001
Deviation by tissue (% vs R100)				
Bone		9.69	9.61	8.88
Liver		6.10	6.78	6.02
Lymphatic nodes		5.54	5.59	4.78
Other visceral tissues		16.63	16.65	15.39

For metabolic measurements related to [^{68}Ga]PSMA (Table VII), no significant difference in SUVmax was observed for an acquisition time at 75% of the usual duration. However, when applying denoising, a significant decrease was noted for S75 images: -0.69 (-11.46%, $p < 0.0001$) and S50 images: -0.44 (-9.79%, $p < 0.0001$) for SUVmax. Although SUVmax values varied slightly after denoising, the differences remained minimal, with stable standard deviations and low coefficients of variation across reconstructions (CV range: 0.623–0.87 for [^{18}F]FDG and 0.606–1.20 for [^{68}Ga]PSMA). Size effects were negligible (Cohen's d between –0.08 and 0.01), confirming the consistency of SUVmax measurements across protocols (Table VIII, in the appendix).

3. Radiomics analysis

Following the semi-quantitative analysis, 162 radiomic features were evaluated to assess the reproducibility of complex image characteristics and the potential for using denoised and non-denoised images in combination. The distribution of CCC values showed that most radiomic features had high reproducibility across reconstructions for both [^{18}F]FDG and [^{68}Ga]PSMA, with CCC values clustering above 0.95 (Figure 8).

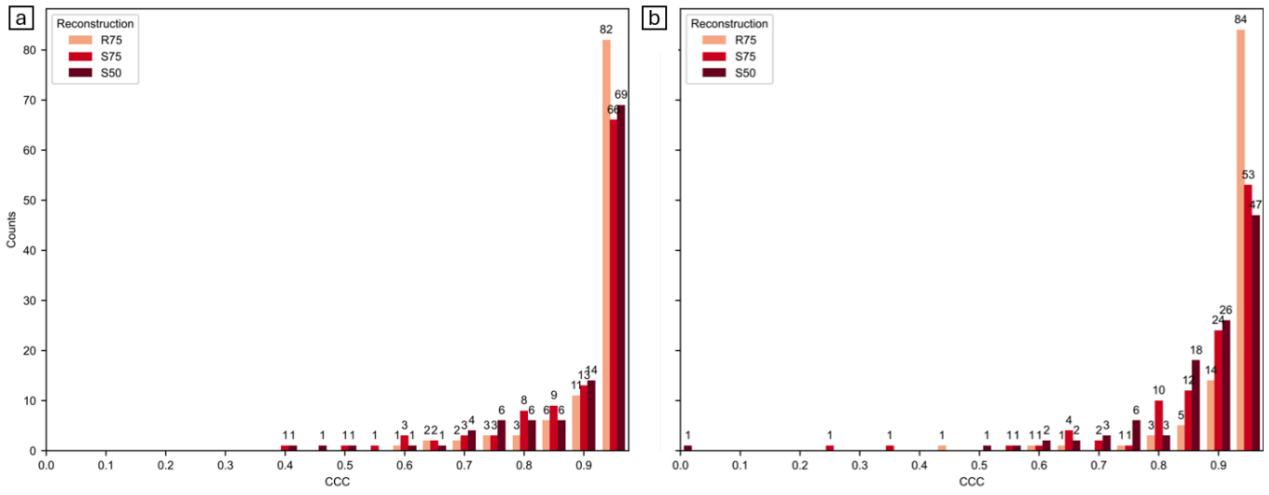


Fig. 8 Distribution of concordance correlation coefficient (CCC) values for radiomic features extracted from [^{18}F]FDG (a) and [^{68}Ga]PSMA (b).

All CCC values for all radiomics features and for [^{18}F]FDG and [^{68}Ga]PSMA radiotracers are available in Online Resource 2. Only a small proportion of features showed poor agreement (CCC < 0.8), with 14.3% for [^{18}F]FDG and 15.2% for [^{68}Ga]PSMA in S50.

Regarding radiomic features with lower concordance, Figure 9 shows the number of radiomic features with a CCC below 0.8 when comparing native and AI-denoised PET/CT images. The most affected radiomic features belonged to the intensity-based (INTENSITY) and gray level size zone matrix (GLSZM) categories, particularly after denoising at 75% and 50% acquisition times (S75 and S50). In contrast, features derived from the gray level co-occurrence matrix (GLCM), gray level run length matrix (GLRLM), morphological descriptors, and neighborhood gray tone difference matrix (NGTDM) remained largely stable. When analysed by radiotracer, [^{18}F]FDG showed a slightly higher number of affected features (n = 37) compared to [^{68}Ga]PSMA (n = 31). The effect of reduced acquisition time alone (R75) was limited, whereas the application of AI-based denoising (S75 and S50) resulted in a greater number of features with degraded reproducibility, especially for [^{18}F]FDG .

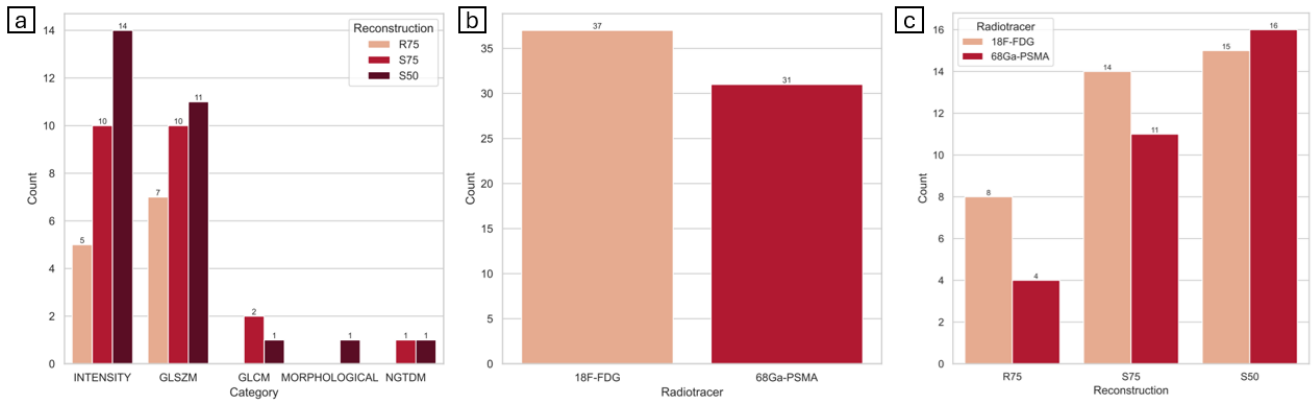


Fig. 9 Number of radiomic features with CCC < 0.8 per feature category (a), per radiotracer (b), and per reconstruction type (c) when comparing native and AI-denoised PET/CT images.

Fifteen radiomic features showed weaker correlation for both radiotracers (Table IX). Notably, denoising did not improve the CCC of these features and even tended to degrade it, particularly

for metrics related to intensity variability, low-intensity zones, small zone sizes, or high homogeneity. Some radiomic features were impacted in terms of CCC for only one of the two radiotracers used in the study.

Table IX Most impacted radiomic characteristics (CCC < 0.8) for [^{18}F]FDG and [^{68}Ga]PSMA.

Radiomic characteristics	**[^{18}F]FDG**			**[^{68}Ga]PSMA**		
GLRLM	**R75**	**S75**	**S50**	**R75**	**S75**	**S50**
LongRunLowGreyLevelEmphasis(IBSI :IVPO)	0.964	0.692	0.769	0.99	0.887	0.797
LongRunsEmphasis(IBSI :W4KF)	0.969	0.723	0.854	0.99	0.847	0.785
LargeZoneEmphasis(IBSI :48P8)	0.8	0.808	0.83	0.985	0.687	0.761
LargeZoneLowGreyLevelEmphasis(IBSI :YH51)	0.752	0.516	0.485	0.994	0.659	0.723
NormalisedGreyLevelNonUniformity(IBSI :Y1RO)	0.754	0.659	0.743	0.601	0.591	0.848
SmallZoneEmphasis(IBSI :5QRC)	0.669	0.761	0.768	0.866	0.809	0.766
SmallZoneLowGreyLevelEmphasis(IBSI :5RAI)	0.671	0.577	0.439	0.688	0.386	0.505
INTENSITY-BASED						
IntensityBasedCoefficientOfVariation(IBSI:7TET)[SUVbw]	0.784	0.657	0.735	0.769	0.802	0.601
IntensityBasedQuartileCoefficientOfDispersion(IBSI:9S40)[SUVbw]	0.835	0.654	0.712	0.819	0.751	0.752
IntensityKurtosis(IBSI:IPH6)[SUVbw]	0.932	0.831	0.777	0.844	0.714	0.805
IntensityHistogramCoefficientOfVariation(IBSI:CWYJ)[Intensity]	0.801	0.679	0.741	0.813	0.83	0.63
IntensityHistogramKurtosis(IBSI:C3I7)[Intensity]	0.93	0.79	0.742	0.832	0.709	0.755
IntensityHistogramQuartileCoefficientOfDispersion(IBSI:SLWD)[Intensity]	0.662	0.458	0.514	0.451	0.241	-0.048
IntensityHistogramSkewness(IBSI:88K1)[Intensity]	0.935	0.751	0.797	0.862	0.776	0.54
NGTDM						
Busyness(IBSI :NQ30)	0.866	0.806	0.611	0.891	0.68	0.94

For [^{18}F]FDG, the features showing reduced concordance when comparing native images to those denoised by an AI-based algorithm are listed in Table X. These include GLCM and morphological-based metrics, such as texture regularity (AngularSecondMoment), grey-level randomness (SumEntropy), and spatial dispersion of uptake (CentreOfMassShift). Radiomic features showing the greatest degradation in CCC exclusively for the [^{68}Ga]PSMA radiotracer are listed in Table XI. These include GLSZM and intensity-based features, such as the size and intensity of homogeneous zones (LargeZoneHighGreyLevelEmphasis, LowGrayLevelZoneEmphasis, ZoneSizeVariance) and the asymmetry of SUV distribution (IntensitySkewness).

Table X Most impacted radiomic characteristics (CCC < 0.8) only for [18F]FDG.

Radiomic characteristics	R75	S75	S50
GLCM			
AngularSecondMoment(IBSI :8ZQL)	0.98	0.743	0.838
SumEntropy(IBSI :P6QZ)	0.897	0.825	0.795
MORPHLOGICAL			
CentreOfMassShift(IBSI:KLMA)[mm]	0.893	0.842	0.8

Table XI Most impacted radiomic characteristics (CCC < 0.8) only for [^{68}Ga]PSMA.

Radiomic characteristics	R75	S75	S50
GLSZM			
LargeZoneHighGreyLevelEmphasis(IBSI :J17V)	0.889	0.626	0.73
LowGrayLevelZoneEmphasis(IBSI :XMSY)	0.959	0.879	0.754
ZoneSizeVariance(IBSI :3NSA)	0.961	0.683	0.661
INTENSITY-BASED			
IntensitySkewness(IBSI:KE2A)[SUVbw]	0.904	0.776	0.621

DISCUSSION

The aim of this study was to evaluate whether a reduction in acquisition time, combined with AI-based denoising, could preserve image quality, semi-quantitative accuracy, and radiomic feature stability in PET/CT imaging using both [^{18}F]FDG and [^{68}Ga]PSMA tracers.

Our findings, confirmed both on standardised phantoms and in clinical conditions, are consistent with previously published results, showing a decrease in SUV-based measurements but an improvement in overall qualitative image assessment. Importantly, this is the first study to demonstrate these effects simultaneously for both [^{18}F]FDG and [^{68}Ga]PSMA within the largest cohort to date. Finally, we report for the first time a high level of concordance between radiomic features extracted from native and denoised images, despite acquisition time reduction, thus supporting the robustness of radiomics in such optimised imaging protocols.

In contrast to Bonardel et al. (10), our phantom analysis showed no significant alteration in contrast for R75 and S75 images, possibly due to differences in acquisition time or imaging system. However, consistent with their findings, denoising markedly reduced background noise variability in shortened acquisitions. Clinically, image quality and noise levels in S75 images were comparable with native R100 images across all the criteria assessed. Only clinician confidence remained significantly lower for SubtlePET®-processed images, possibly due to reduced familiarity with AI-modified reconstructions and the appearance of some artifacts. These results are consistent with the existing literature (6,17), particularly with the study by K. Weyts, which did not identify any significant differences in the image quality index between images acquired with a 90-second step and those acquired with a 45-second step processed by AI (score rated as "good" in 92% of cases and "moderate" in 8%, $p = 0.8$). Furthermore, K. Katsari (2) demonstrated a score of 4.62 for denoised images compared to 4.54 for native images. The PCA reflecting clinical and technical features show a marked reduction in inter-observer distances in denoised images for technical features, with no impact on the clinical

component. This suggests better convergence in technical evaluations, likely caused by effective enhancement by SubtlePET®, while subjective heterogeneity persisted in clinical assessments. A significant change in metabolic values was observed, with significantly lower SUVmax in images with reduced acquisition time or post-processed compared to native images, particularly in denoised images (up to -7.73% in [^{18}F]FDG and -11.46% in [^{68}Ga]PSMA). This decrease in metabolic values has also been reported in several other studies, including that of K. Katsari (2), where the mean SUVmax decreased from 11.4 to 9.8 between AI-non-processed images and AI-processed images. Despite minor variations in SUVmax after denoising, the consistency of the measurements across reconstructions was confirmed by low coefficients of variation, reinforcing their reliability for semi-quantitative analysis.

One of the main contributions of our study is the exploration of changes in radiomic features, an aspect that remains underexplored in the current literature. Until now, this topic had only been addressed in an experimental setting, in the study by Jaudet et al. (18), which compared images reconstructed with and without the SubtlePET® software, without applying a reduction in acquisition time or injected dose. Our study demonstrates an excellent correlation between radiomic features from native and denoised images with [^{18}F]FDG and [^{68}Ga]PSMA, consistent with the previous study, which reported a CCC > 0.85 for 86.5% of the features. We observed an increase in the number of radiomic features impacted after denoising, particularly in denoised reconstructions with 15 features for [^{18}F]FDG and 16 for [^{68}Ga]PSMA in the S50 reconstruction, compared to only 8 and 4 features respectively in the R75. Among the most impacted radiomic features (CCC < 0.8), those with the lowest concordance were primarily related to intensity and textural heterogeneity. The lowest CCC values were observed for GLSZM_LargeZoneLowGreyLevelEmphasis, GLSZM_SmallZoneLowGreyLevelEmphasis, and intensity-histogram_IntensityHistogramQuartileCoefficientOfDispersion. These features are particularly sensitive to modifications in low grey-level and small homogeneous zones. The

degradation in reproducibility may be attributed to the smoothing effect introduced by AI-based denoising, which increases global image homogeneity and may artificially reduce textural variability in small or low-intensity regions. Other features, such as GLRLM_LongRunLowGreyLevelEmphasis and NGTDM_Busyness, also showed reduced concordance, reflecting the complex impact of denoising on spatial and statistical texture properties. These findings support the integration of novel images into international databases, while underscoring the need for caution due to reduced concordance in some radiomic features.

Nevertheless, our study has several limitations. First, it relies on a single imaging system (Philips VEREOS) and was conducted at a single centre, which may limit the generalisability of the results. Regarding the study population, although a substantial number of patients were included in the overall analysis, subgroup analyses were based on smaller cohorts, particularly for patients with BMI > 35 and those undergoing [^{68}Ga]PSMA imaging. It is important to highlight that, to date, the only prior study investigating the impact of denoising software on [^{68}Ga]PSMA imaging was retrospective in design and included 30 patients (8). Selecting the lesions to be analysed in each scan was left to the discretion of the clinician. It is also possible that prior knowledge of the image processing method may have influenced clinicians' subjective assessment of lesion quality and overall scan interpretation. Regarding radiomics analysis, only segmentation based on maximum intensity was used, although several studies have shown a significant impact of the segmentation method on the features extracted (19). A different segmentation approach, such as one based on adaptive thresholds or active contour methods, may have altered the values of the features extracted. Moreover, the lack of external validation on different PET/CT systems and protocols remains a limitation regarding the transferability of the results.

These results highlight the potential for integrating AI-based denoising into clinical PET workflows, particularly to make it possible to reduce acquisition times or doses without compromising image quality or radiomic robustness, despite a known impact on semi-

quantitative metrics. The preservation of most radiomic features across reconstruction methods supports the feasibility of combining denoised and non-denoised datasets to expand the pool of data available for radiomics research. However, further studies are needed to confirm these findings in larger cohorts, especially for [^{68}Ga]PSMA, and to assess the impact of denoising on other radiotracers such as [^{68}Ga]DOTATOC and [^{18}F]DOPA. Altogether, these findings support the safe and robust use of AI-denoised PET/CT in clinical and research applications, with careful consideration for the behaviour of specific radiomic features.

CONCLUSION

Our prospective clinical study conducted on a large cohort reinforces the value of AI-based denoising software in improving the quality of PET/CT examinations performed with reduced acquisition times. Furthermore, we demonstrate the preservation of a strong correlation between radiomic features extracted from denoised images and those from native images, thereby supporting their potential integration into radiomic research.

BIBLIOGRAPHY

1. Guignard R, Cimarelli S, Fernandez V, Geffroy B. Dynamique de l'innovation en médecine nucléaire : une décennie propice pour la diffusion de la TEP. Médecine Nucléaire. juill 2021;45(4):206.

2. Katsari K, Penna D, Arena V, Polverari G, Ianniello A, Italiano D, et al. Artificial intelligence for reduced dose 18F-FDG PET examinations: a real-world deployment through a standardized framework and business case assessment. EJNMMI Phys. déc 2021;8(1):25.

3. Koopman D, Van Dalen JornA, Stevens H, Slump CH, Knollema S, Jager PL. Performance of Digital PET Compared with High-Resolution Conventional PET in Patients with Cancer. J Nucl Med. oct 2020;61(10):1448-54.

4. Teoh EJ, McGowan DR, Macpherson RE, Bradley KM, Gleeson FV. Phantom and Clinical Evaluation of the Bayesian Penalized Likelihood Reconstruction Algorithm Q.Clear on an LYSO PET/CT System. J Nucl Med. sept 2015;56(9):1447-52.

5. Ruan W, Qin C, Liu F, Pi R, Gai Y, Liu Q, et al. Q.Clear reconstruction for reducing the scanning time for 68 Ga-DOTA-FAPI-04 PET/MR imaging. Eur J Nucl Med Mol Imaging. juin 2023;50(7):1851-60.

6. Weyts K, Lasnon C, Ciappuccini R, Lequesne J, Corroyer-Dulmont A, Quak E, et al. Artificial intelligence-based PET denoising could allow a two-fold reduction in [18F]FDG PET acquisition time in digital PET/CT. Eur J Nucl Med Mol Imaging. sept 2022;49(11):3750-60.

7. Xu J, Gong E, Pauly J, Zaharchuk G. 200x Low-dose PET Reconstruction using Deep Learning [Internet]. arXiv; 2017 [cité 30 déc 2023]. Disponible sur: http://arxiv.org/abs/1712.04119

8. Margail C, Merlin C, Billoux T, Wallaert M, Otman H, Sas N, et al. Imaging quality of an artificial intelligence denoising algorithm: validation in 68Ga PSMA-11 PET for patients with biochemical recurrence of prostate cancer. EJNMMI Res. 25 mai 2023;13(1):50.

9. Muzaffar R, Christopher K, Frye R, Sterkel B, Gandhi H, Gulaka P, et al. Impact of AI on Image Quality and SUV Quantification on F18-FDG PET/CT . J Nucl Med. 1 mai 2020;61(supplement 1):1479.

10. Bonardel G, Dupont A, Decazes P, Queneau M, Modzelewski R, Coulot J, et al. Clinical and phantom validation of a deep learning based denoising algorithm for F-18-FDG PET images from lower detection counting in comparison with the standard acquisition. EJNMMI Phys. déc 2022;9(1):36.

11. Burton C. SubtlePET Analysis Using American College of Radiology Phantom and Guidelines. J Nucl Med. 1 août 2022;63(supplement 2):3290.

12. De Summa M, Ruggiero MR, Spinosa S, Iachetti G, Esposito S, Annunziata S, et al. Denoising approaches by SubtlePET^{TM} artificial intelligence in positron emission tomography (PET) for clinical routine application. Clinical and Translational Imaging. 2024;1-10.

13. Carles M, Fechter T, Martí-Bonmatí L, Baltas D, Mix M. Experimental phantom evaluation to identify robust positron emission tomography (PET) radiomic features. EJNMMI Phys. déc 2021;8(1):46.

14. Pfaehler E, Beukinga RJ, De Jong JR, Slart RHJA, Slump CH, Dierckx RAJO, et al. Repeatability of ^{18}F- FDG PET radiomic features: A phantom study to explore sensitivity to image reconstruction settings, noise, and delineation method. Medical Physics. févr 2019;46(2):665-78.

15. Vallières M, Zwanenburg A, Badic B, Cheze Le Rest C, Visvikis D, Hatt M. Responsible Radiomics Research for Faster Clinical Translation. J Nucl Med. févr 2018;59(2):189-93.

16. Nioche C, Orlhac F, Boughdad S, Reuzé S, Goya-Outi J, Robert C, et al. LIFEx: A Freeware for Radiomic Feature Calculation in Multimodality Imaging to Accelerate Advances in the Characterization of Tumor Heterogeneity. Cancer Research. 15 août 2018;78(16):4786-9.

17. Le V, Frye S, Botkin C, Christopher K, Gulaka P, Sterkel B, et al. Effect of PET Scan with Count Reduction Using AI-Based Processing Techniques on Image Quality. J Nucl Med. 1 mai 2020;61(supplement 1):3095.

18. Jaudet C, Weyts K, Lechervy A, Batalla A, Bardet S, Corroyer-Dulmont A. The Impact of Artificial Intelligence CNN Based Denoising on FDG PET Radiomics. Front Oncol. 24 août 2021;11:692973.

19. Lovinfosse P, Visvikis D, Hustinx R, Hatt M. FDG PET radiomics: a review of the methodological aspects. Clin Transl Imaging. oct 2018;6(5):379-91.

20. Hricak H, Ward ZJ, Atun R, Abdel-Wahab M, Muellner A, Scott AM. Increasing Access to Imaging for Addressing the Global Cancer Epidemic. Radiology. déc 2021;301(3):543-6.

21. NHS England. Diagnostic Imaging Dataset 2020–21 Data. NHS England; 2021.

22. Denton K, Haider I, Hill J, Hunt SL, Ash R. Of Mice and Roentgen: Radiologist Satisfaction with a Non-conventional 13-Button Mouse—One Institution's Experience. J Digit Imaging. déc 2018;31(6):776-82.

23. Siemens Healthineers. syngo.via WebViewer Operator Manual – Web Client VA20B [Internet]. Siemens Healthineer; 2020. Disponible sur: https://doclib.siemens-healthineers.com/rest/v1/view?document-id=781320&utm_source=chatgpt.com

24. Drew T, Williams LH, Aldred B, Heilbrun ME, Minoshima S. Quantifying the costs of interruption during diagnostic radiology interpretation using mobile eye-tracking glasses. J Med Imag. 2 mars 2018;5(03):1.

25. Lidén M, Andersson T, Geijer H. Alternative User Interface Devices for Improved Navigation of CT Datasets. J Digit Imaging. févr 2011;24(1):126-34.

26. Sherbondy AJ, Holmlund D, Rubin GD, Schraedley PK, Winograd T, Napel S. Alternative Input Devices for Efficient Navigation of Large CT Angiography Data Sets. Radiology. févr 2005;234(2):391-8.

27. Gegenfurtner A, Lehtinen E, Säljö R. Expertise Differences in the Comprehension of Visualizations: a Meta-Analysis of Eye-Tracking Research in Professional Domains. Educ Psychol Rev. déc 2011;23(4):523-52.

28. Brunyé TT, Drew T, Weaver DL, Elmore JG. A review of eye tracking for understanding and improving diagnostic interpretation. Cogn Research. déc 2019;4(1):7.

29. Brunyé TT, Nallamothu BK, Elmore JG. Eye-tracking for assessing medical image interpretation: A pilot feasibility study comparing novice vs expert cardiologists. Perspect Med Educ. 11 avr 2019;8(2):65-73.

30. Borys M, Plechawska-Wójcik M. Eye-tracking metrics in perception and visual attention research. EJMT. 2017;3:11-23.

31. Rayner K. Eye movements in reading and information processing: 20 years of research. Psychological Bulletin. 1998;124(3):372-422.

32. Leveque L, Bosmans H, Cockmartin L, Liu H. State of the Art: Eye-Tracking Studies in Medical Imaging. IEEE Access. 2018;6:37023-34.

33. Bertram R, Kaakinen J, Bensch F, Helle L, Lantto E, Niemi P, et al. Eye Movements of Radiologists Reflect Expertise in CT Study Interpretation: A Potential Tool to Measure Resident Development. Radiology. déc 2016;281(3):805-15.

34. Gegenfurtner A, Lehtinen E, Säljö R. Expertise Differences in the Comprehension of Visualizations: a Meta-Analysis of Eye-Tracking Research in Professional Domains. Educ Psychol Rev. déc 2011;23(4):523-52.

35. Ji Y, Kong Z, Deng Y, Chen J, Liu Y, Zhao L. The role of eye tracker in teaching video-assisted thoracoscopic surgery: the differences in visual strategies between novice and expert surgeons in thoracoscopic surgery. Ann Transl Med. mai 2022;10(10):592-592.

36. Waite S, Kolla S, Jeudy J, Legasto A, Macknik SL, Martinez-Conde S, et al. Tired in the Reading Room: The Influence of Fatigue in Radiology. Journal of the American College of Radiology. févr 2017;14(2):191-7.

37. Donovan T, Litchfield D. Looking for Cancer: Expertise Related Differences in Searching and Decision Making. Applied Cognitive Psychology. janv 2013;27(1):43-9.

38. Brunyé TT, Drew T, Kerr KF, Shucard H, Weaver DL, Elmore JG. Eye tracking reveals expertise-related differences in the time-course of medical image inspection and diagnosis. J Med Imag [Internet]. 27 oct 2020 [cité 17 sept 2025];7(05). Disponible sur: https://www.spiedigitallibrary.org/journals/journal-of-medical-imaging/volume-7/issue-05/051203/Eye-tracking-reveals-expertise-related-differences-in-the-time-course/10.1117/1.JMI.7.5.051203.full

39. Balint BJ, Steenburg SD, Lin H, Shen C, Steele JL, Gunderman RB. Do Telephone Call Interruptions Have an Impact on Radiology Resident Diagnostic Accuracy? Academic Radiology. déc 2014;21(12):1623-8.

40. Wynn RM, Howe JL, Kelahan LC, Fong A, Filice RW, Ratwani RM. The Impact of Interruptions on Chest Radiograph Interpretation. Academic Radiology. déc 2018;25(12):1515-20.

SUPPLEMENTARY INFORMATION

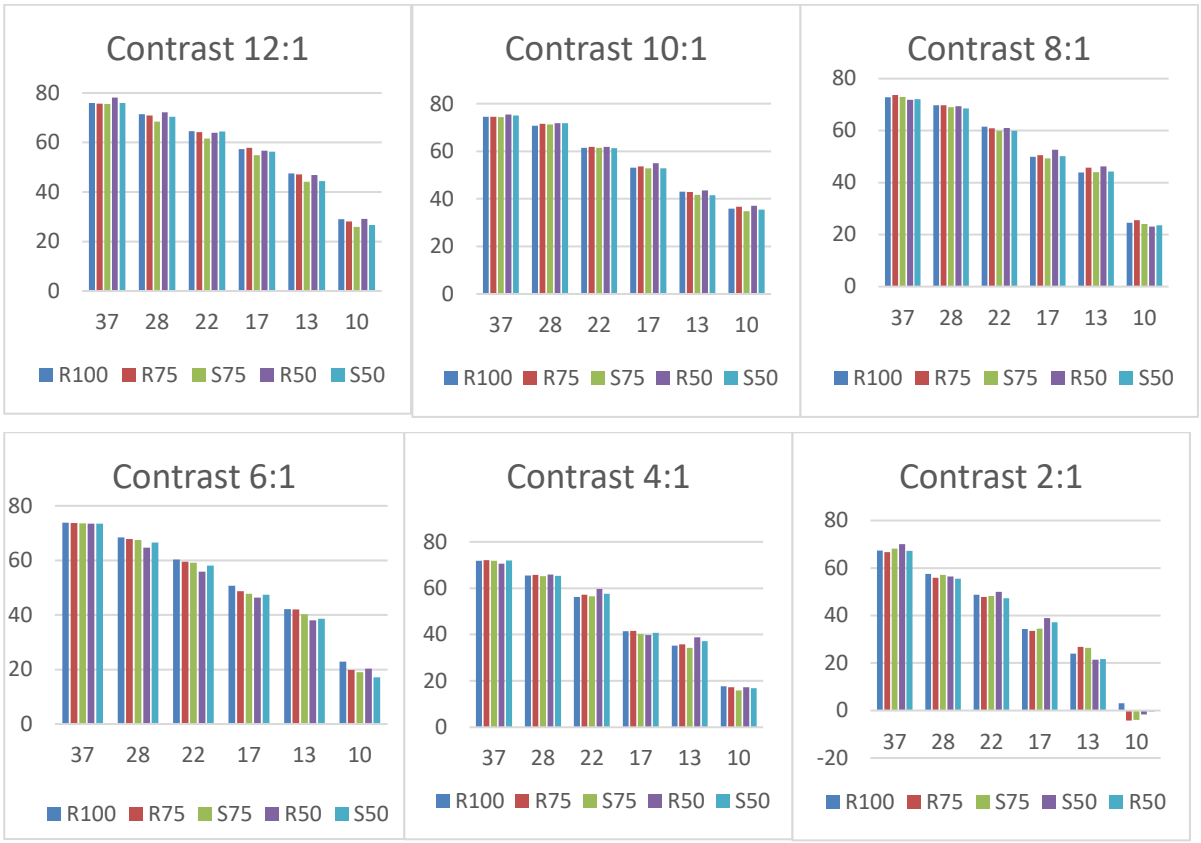
Table II Mean inter-observer distances and standard deviations along technical (PC1: global noise, liver heterogeneity, liver image quality, whole-body image quality) and clinical (PC2: interpretation speed, diagnostic confidence) axes for each reconstruction protocol.

Reconstruction	Dimension	Mean distance	Standard deviation PC1	Standard deviation PC2
R100	**Technic**	1.218	0.938	0.084
R100	**Clinic**	0.665	0.481	0.088
R75	**Technic**	1.384	1.026	0.155
R75	**Clinic**	0.609	0.436	0.082
S75	**Technic**	0.686	0.497	0.089
S75	**Clinic**	0.595	0.429	0.062
S50	**Technic**	1.361	0.926	0.216
S50	**Clinic**	0.698	0.503	0.108

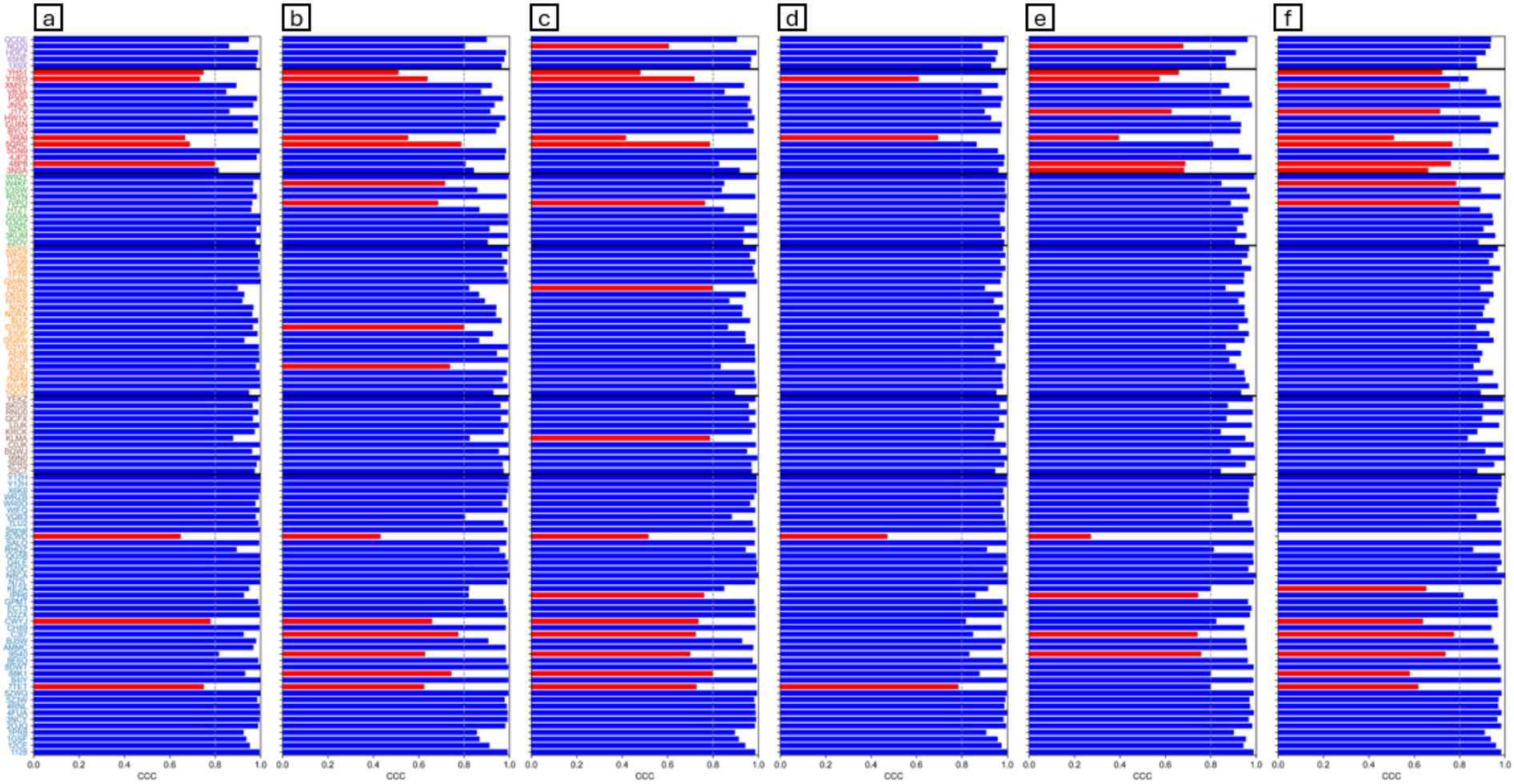
Table VIII Standard deviation, and coefficient of variation (CV) for SUVmax ratios across reconstruction protocols, for [^{18}F]FDG and [^{68}Ga]PSMA.

	[^{18}F]FDG				[^{68}Ga]PSMA			
	Reconstruction	**Standard deviation**	**CV**	**Cohen's d**	**Reconstruction**	**Standard deviation**	**CV**	**Cohen's d**
SUVmax	R100	5.37	0.83	0	R100	11.42	1.17	0
	R75	4.33	0.81	0.01	R75	11.23	1.15	0.003
	S75	4.31	0.87	-0.07	S75	10.87	0.606	-0.08
	S50	4.30	0.623	-0.06	S50	10.75	1.20	-0.07

ONLINE RESOURCE



Resource 1. Variation of sphere-to-background contrast (%) according to acquisition time (R100, R75) and AI-based denoising (S75, S50) across the six phantom contrast conditions.



Resource 2. Concordance correlation coefficients (CCC) of radiomic features between R100 and denoised reconstructions for [^{18}F]FDG (a–c) and [^{68}Ga]PSMA (d–f): (a, d) R75, (b, e) S75, (c, f) S50. Features are colour-coded by class: intensity (blue), morphology (brown), GLCM (orange), GLRLM (green), GLSZM (red), and NGTDM (purple).

INNOVATIVE EVALUATION OF A NON-CONVENTIONAL MOUSE FOR IMAGE INTERPRETATION IN METABOLIC IMAGING: INTEGRATION OF EYE TRACKING, KINEMATIC ANALYSIS, AND QUALITATIVE FEEDBACK

A Dambrain[1], C Bouron[2], Jane Loh[3], PJ Mention[2], N Alarion[4], K Cohen Tannugi[5], M Decagny[2], PA Dufour[6], H Rakotonirina[2], O Morel[6], S Girault[6], C Guillerminet[8], E Gontier[4], C Cavaro-Menard[7], F Lacoeuille[9]

1. MD University Hospital of Angers, INSERM, CNRS, CRCI(2)NA, F-49000, Angers, France ; CHU Angers, University of Angers, F-49000, Angers, France
2. MD, University Hospital of Angers, France
3. Independent Epidemiologist, Le Mans, France
4. MD, Imagerie moléculaire et théranostique group (IMT), Asterion network, Le Mans, France
5. MD, Le Mans Hospital, Le Mans, France
6. MD, Institut de Cancérologie de l'Ouest (ICO), Angers, France
7. University of Angers, LARIS, SFR MATHSTIC, F-49000 Angers, France
8. Medical physicist, Department of Medical Physics, Institut de Cancérologie de l'Ouest (ICO), Paul Papin Center, Angers, France
9. PharmD, PhD, University Hospital of Angers, INSERM, CNRS, CRCI(2)NA, F-49000, Angers, France ; CHU Angers, University of Angers, F-49000, Angers, France

ABSTRACT

ABSTRACT

Purpose: To evaluate the impact of a non-conventional mouse on PET/CT interpretation, using eye-tracking, mouse kinematics, and ergonomic assessment.

Materials and methods: In this prospective, multicenter study, ten physicians (2 residents and 8 specialists) interpreted fourteen standardized PET/CT examinations using both a standard three-button mouse and a non-conventional mouse (RAZER Naga Pro). Eye-tracking metrics, mouse dynamics, and shortcut use were recorded. Ergonomic perception was assessed with a Likert-scale questionnaire. Analyses were performed with mixed models adjusted for physician and examination duration.

Results: Compared with the standard mouse, the non-conventional mouse significantly reduced the number of fixations (571 vs. 635; $p = 0.004$) and their total duration (220 vs. 242 s; $p = 0.035$). The number of saccades was also lower ($p<0.01$), while their mean duration tended to increase. Mouse kinematics showed reductions in maximum and mean movement speed and in distance travelled ($p <0.05$). The number of executed shortcuts was lower with the non-conventional mouse (e.g., windowing changes: 35 vs. 49, $p = 0.013$; left clicks: 171 vs. 213, $p = 0.013$). Qualitative evaluation favored the non-conventional mouse across ergonomics, accessibility, and interpretation comfort (mean 4.5/5 vs. 3.6/5; $p = 0.02$). Global satisfaction increased after testing, reaching 100% versus <40% for the standard mouse.

Conclusion: The non-conventional mouse optimizes visual exploration, reduces redundant cursor movements, and improves ergonomic comfort in PET/CT interpretation. These findings support the integration of specialized pointing devices

Keys Words: Eye tracking, PET/CT, computer mouse, workstation, ergonomic

INTRODUCTION

Over the past decade, the use of positron emission tomography (PET) has markedly increased worldwide, underscoring its growing importance in medical diagnosis and patient management (20,21). Following reconstruction, images are archived in the Picture Archiving and Communication System (PACS) and subsequently reviewed by the nuclear medicine physician, who adjusts the display settings and performs both morphological and metabolic assessments, including measurements of Standardized Uptake Value (SUV) and lesion diameters. These operations are most commonly performed with a standard three-button mouse, which enables users to scroll through image series and focus on specific regions (22). The keyboard offers access to a wide range of shortcuts, but these are often complex and dispersed (23), requiring a dedicated hand and thereby restricting the simultaneous performance of other tasks, such as voice dictation. Even for experienced users, many of these shortcuts still necessitate visual confirmation, thereby interrupting the analysis workflow and potentially causing a loss of concentration, wasted time, or errors (24).

To enhance the ergonomics of interpretation tools, several alternative devices have been proposed, including miniature auxiliary keyboards and non-conventional mice with customizable buttons (25,26). This kind of mouse may provide more direct and intuitive access to interpretation functions, enabling users to maintain uninterrupted visual focus on the screen, thereby promoting continuity of diagnostic analysis and improving comfort during prolonged use. The effectiveness of interpretation tasks can be objectively assessed through eye tracking, which identifies three key phases: search, recognition, and decision-making (27). This method relies on the analysis of fixations – during which diagnostic information is extracted – and saccades, which are rapid eye movements that shift the point of fixation but contribute to minimally cognitive processing (28–30). Investigating these parameters provides valuable insight into error mechanisms and serves as a relevant tool to optimize diagnostic

performance. To date, no studies have evaluated the impact of non-conventional mice in nuclear medicine, nor the influence of the interpretation device on visual search patterns. The only available study, conducted on 59 radiologists and limited to a qualitative assessment, reported a clear preference for non-conventional mice, which were perceived as more precise and efficient (22).

The objective of this study is to compare the use of a standard computer mouse with a non-conventional mouse during the interpretation of 14 standardized examinations. We first analyzed variations in eye-tracking patterns, followed by quantitative data on mouse movements for both devices, and finally assessed their perceived ergonomics. We hypothesize that the non-conventional mouse facilitates a more efficient visual search pattern, more precise movements, fewer shortcut-related errors, and improved user comfort.

MATERIALS AND METHODS

1. Medical study population

This study was approved by the ethics committee of the University Hospital of Angers (meeting of April 8, 2025, approval number 2025-100) and was declared to the CNIL (reference AR25-0105v0). It was conducted prospectively across four centers between June and September 2025 to reflect the heterogeneity of nuclear medicine practices: the University Hospital of Angers, the Institut de cancérologie de l'ouest (ICO, cancer center), the Hospital of Le Mans, and the Imagerie moléculaire et théranostique group, Asterion network (IMT). Ten participants were included, comprising of eight nuclear medicine physicians and two residents, aged between 26 and 59 years. Physicians from the University Hospital of Angers and the Institut de Cancérologie de l'Ouest had no prior experience with non-conventional mice, whereas those from the IMT and the Hospital of Le Mans were regular users. To ensure optimal assessment and minimise the effect of familiarisation, before the evaluation phase, each clinician used the device they were not accustomed to for at least 20 hours under real clinical conditions

2. Materials

2.1. Computer mouse

The non-conventional mouse selected was the Naga Pro (RAZER®), equipped with 12 programmable side buttons and 7 top buttons (Fig. **1**). It provides a maximum sensitivity of 20,000 dots per inch (DPI) through an optical sensor. Data transmission can be achieved via Bluetooth, 2.4 GHz radio frequency, or a wired connection via USB-A. This model was chosen because it was already in routine use at the Centre interregional de lutte contre le cancer and Le Mans Hospital. It was connected in wired mode in accordance with the practices of these centers.

The standard mouse was a wired Lenovo model, connected via USB-A and equipped with 3 top buttons (left click, right click, and clickable scroll wheel). Its optical resolution was approximately 1000 DPI. The keyboard used was also a Lenovo model, with the native shortcuts of the Syngo.Via interpretation software (version 6), summarized in Table I. All clinicians received prior training on the use of both types of equipment before the beginning of the study, supplemented by a summary sheet available for consultation during the training phase. All settings and shortcuts were identical for each participant.

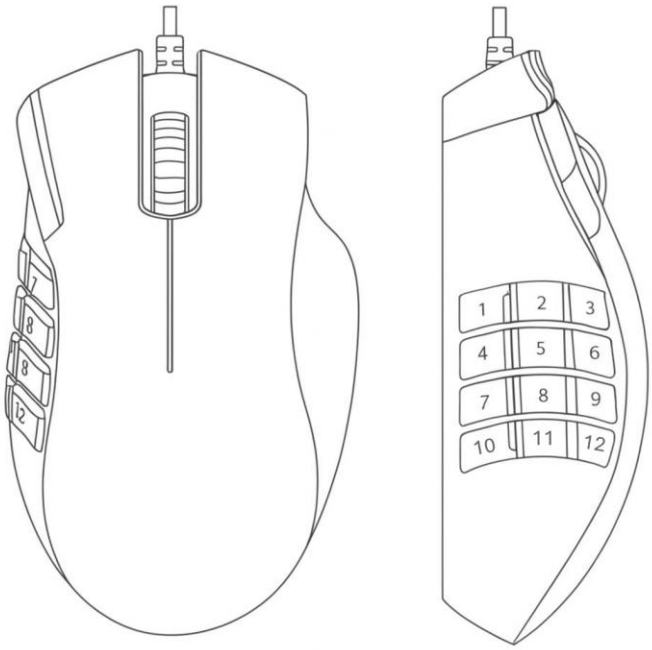


Fig. 1 Schematic representation of a non-conventional mouse showing top and lateral views, with 12 programmable side buttons numbered 1 to 12

Table I Keyboard and non-conventional mouse shortcuts according to the intended action

Keyboard shortcut	Button mouse shortcut	Action
F5	1	Soft tissue window
F6	4	Pulmonary parenchymal window
F7	7	Bone window
F8	12	Brain window
V	2	Volume of interest
D	5	Distance measurement

2.2. Eye Tracker

The eye tracker used was the SMI RED250 system (Remote Eye-tracking Device, SensoMotoric Instruments®), which operates on high-speed infrared videography. The device projects uniform infrared light via light-emitting diodes (LEDs) toward the user, generating a reflection on the anterior corneal surface known as the first Purkinje image, used as a stable reference point. Pupil detection is allowed by its strong absorption of infrared light, which creates a sharp contrast with the cornea. The gaze angle was determined by measuring pupil displacement relative to the corneal reflection. Prior calibration, achieved by fixating on successive targets, allowed the mapping of ocular vectors to screen positions. The system included head-movement compensation to reduce artifacts and operated at a sampling frequency of 250 Hz with an accuracy of approximately 0.5° of visual angle. Eye tracking was performed in real time, and data were analyzed using SMI BeGaze™ software.

3. Quantitative measures

3.1. Study protocol

Fourteen patients with neoplastic disease were divided into two comparable series of seven patients. Each series comprised six pathological examinations (with fewer than three lesions or with multiple lesions) and one normal examination, with the operators blinded to this distribution. Both the allocation of the series to be interpreted with the unconventional mouse and the order of case presentation within each series were randomized. The display configuration was standardized with an axial-slice layout and a uniform color scale (Warm Metal) applied to all examinations. For each examination, metabolic (SUVmax) and morphological measurements (two perpendicular axes for lesions and the short axis for lymph nodes) were performed using the appropriate imaging window. Each lesion was then briefly described, including its location, morphological features, diameter, and SUVmax. This description enabled quality control of the number of lesions detected by the operator.

3.2. Eye-tracking analysis

For the eye-tracking analysis, we selected simple and reproducible parameters that have been consistently reported in the literature as correlating with the different stages of image interpretation and with clinician attention (27,28,30,31). The following metrics were measured: total fixation duration, number of fixations, mean fixation duration, total saccade duration, number of saccades, mean saccade duration, number of gaze exits (gaze outside the screen), and the scan ratio calculated using the formula described below (Equation 1). A saccade is a rapid eye movement that shifts the gaze from one point of interest to another, with minimal visual processing during the movement. A fixation is a period of relative gaze stability on a specific area during which visual information is actively processed, typically lasting more than 100 ms.

$$\text{Scanning coefficient} = \frac{Number\ of\ saccades}{Number\ of\ fixations}$$

Equation 1 Scanning coefficient: ratio between the number of saccades and fixations

3.3. Time analysis

The total time required to perform the measurements was recorded and compared between the standard and the non-conventional mouse. Timing started at the opening of the examination and stopped once the physician judged the interpretation to be complete.

3.4. Mouse Movement Analysis

For both devices, mouse movement parameters and all shortcuts used were recorded with the MiniMicroMouse software (Version 8.3.2.1, TURNSSOFT®) at a sampling frequency of 10 ms. The recorded data included the time interval between two mouse movements, the spatial coordinates of the cursor, and the shortcuts used with either the non-conventional mouse or the keyboard during interpretation.

4. Qualitative Parameters

After the eye-tracking session, each physician completed an evaluation form comparing the standard and non-conventional devices, using a 5-point Likert scale. The assessed criteria included ergonomics (pointer smoothness, ergonomic grip, key responsiveness, haptic feedback), accessibility (window navigation, measurement performance), interpretation comfort (dictation facility, time efficiency, reliability), ease of use (learning curve, ease of handling, button accessibility), as well as overall preference and overall performance. The second part of the evaluation focused on satisfaction before and after the trial period with the different devices.

5. Statistical Analysis

The data were analyzed using R software (version 4.4.1). Quantitative variables were summarized as medians with interquartile ranges (IQR). Comparisons between standard and non-conventional mice were performed using the Wilcoxon rank-sum test. To account for physician-related variability and examination duration, which may directly influence oculographic outcomes, linear mixed-effects models were applied. Device type was included as a fixed effect, while participant and examination duration were modeled as random effects. Results were reported as standardized β coefficients with 95% confidence intervals. Categorical variables (qualitative assessments on a Likert scale) were compared using the Wilcoxon signed-rank test, and p-values were adjusted for multiple testing according to the Benjamini–Hochberg procedure. Statistical significance was defined as $p < 0.05$.

RESULTS

Ten physicians were included in the study: four routinely used a non-conventional device in their daily practice, while six worked with a standard mouse. A total of 140 examinations were analyzed with 14 per physician across both series. No data were missing for eye-tracking metrics, mouse kinematics, shortcut usage, or qualitative assessments. All lesions were consistently detected, interpreted, and reported in the final clinical report by all readers, regardless of the device used (standard or non-conventional mouse). The study cohort included clinicians with experience levels ranging from 1 year to 31 years, including both residents and senior practitioners. The demographic characteristics of the study population, stratified by study site, are summarized in Table II. Both series of examinations were judged to be similar by all participants.

Table II Demographic, professional, and practice-related characteristics of participating physicians by inclusion center: University Hospital Angers (CHU Angers), Institut de Cancerologie de l'Ouest (ICO), Imagerie moléculaire et théranostique *group* (IMT) and Le Mans Hospital (CHM).

	CHU Angers	**ICO**	**IMT**	**CHM**
Number of participants	5	2	2	1
Age in years (min-max)	26-46	36 – 59	42-47	36
Experience (years)	1-18	9-31	18-23	6
Institutional status	University hospital	Oncology center	Private center	Peripheral hospital
Usual device	Standard (1 resident: non-conventional)	Standard	Non-conventional	Non-conventional
Prior use of non-conventional mouse	No : 60% ; Yes : 40%	No : 100%	Yes : 100%	Yes : 100%

1. Eye-tracking Analysis

Table III presents a comparative analysis of eye-tracking parameters between the standard and non-conventional mouse, using both unadjusted and adjusted statistical approaches. The unadjusted analysis, based on the Wilcoxon test, revealed only one significant difference: the number of screen exits was lower with the non-conventional mouse ($p < 0.001$). However, this

difference was no longer significant after adjustment for physician and examination duration. Fixation and saccade parameters showed no significant differences in the unadjusted analysis. In contrast, the adjusted analysis using linear mixed models revealed several significant differences, suggesting a major influence of the interpretation duration, the physician effect, and the habitual use of the device. There was a statistically significant reduction in the number of fixations (571 vs. 634; p = 0.004) and in their total duration (220 vs. 242 s; p = 0.035). The number of saccades was significantly reduced, whereas their mean duration was significantly increased with the non-conventional mouse (p = 0.006 and p = 0.002, respectively). Other parameters, including the mean fixation duration and the total duration of saccades, did not differ significantly between the two experimental conditions. The scanning coefficient showed a significant but minimal increase.

Table III Comparison of eye-tracking parameters between the standard and non-conventional mouse. IQR: interquartile range, s: second, ms: milliseconds, n: number, p-values unadjusted from the Wilcoxon test, and p-values adjusted from the mixed model adjusted for examination duration, familiarity with the device and medical population.

Parameters	Standard mouse median [IQR]	Non-conventional mouse median [IQR]	*p*-value unadjusted	*p*-value adjusted
Total fixation duration (s)	242.69 [183.13–302.03]	220.9 [154.81–301.37]	0.341	**0.035**
Number of fixations (n)	634.75 [435.25–833.5]	571.5 [366.25–873.62]	0.414	**0.004**
Mean fixation duration (ms)	368.04 [308.07–491.19]	375.48 [275.44–496.77]	0.905	0.283
Total saccade duration (s)	17.68 [12.51–32.54]	18.33 [10.74–36.93]	0.814	0.459
Number of saccades (n)	648.75 [442.62–844.38]	581.5 [378.62–874.75]	0.452	**0.006**
Mean saccade duration (ms)	29.89 [24.92–40.38]	31.88 [23.22–45.33]	0.922	**0.002**
Number of gaze exits (n)	24.5 [12–40.38]	9.75 [3.12–26.12]	**<0.001**	0.631
Scanning coefficient	1.01 [0.999–1.03]	1.01 [1.0–1.03]	0.69	**0.004**

To assess the influence of habitual use of a specific device, a subgroup analysis was performed comparing physicians according to their usual equipment, presented in Fig. **2**. In this comparison, physicians accustomed to the non-conventional mouse showed a consistent reduction in the number and total fixation duration, as well as number of saccades when using their usual device, compared with physicians accustomed to the standard mouse using the

standard mouse. In contrast, the number of screen exits was significantly lower with the non-conventional mouse. Total saccade duration did not differ significantly between the two experimental conditions, and the difference in mean saccade duration was no longer significant.

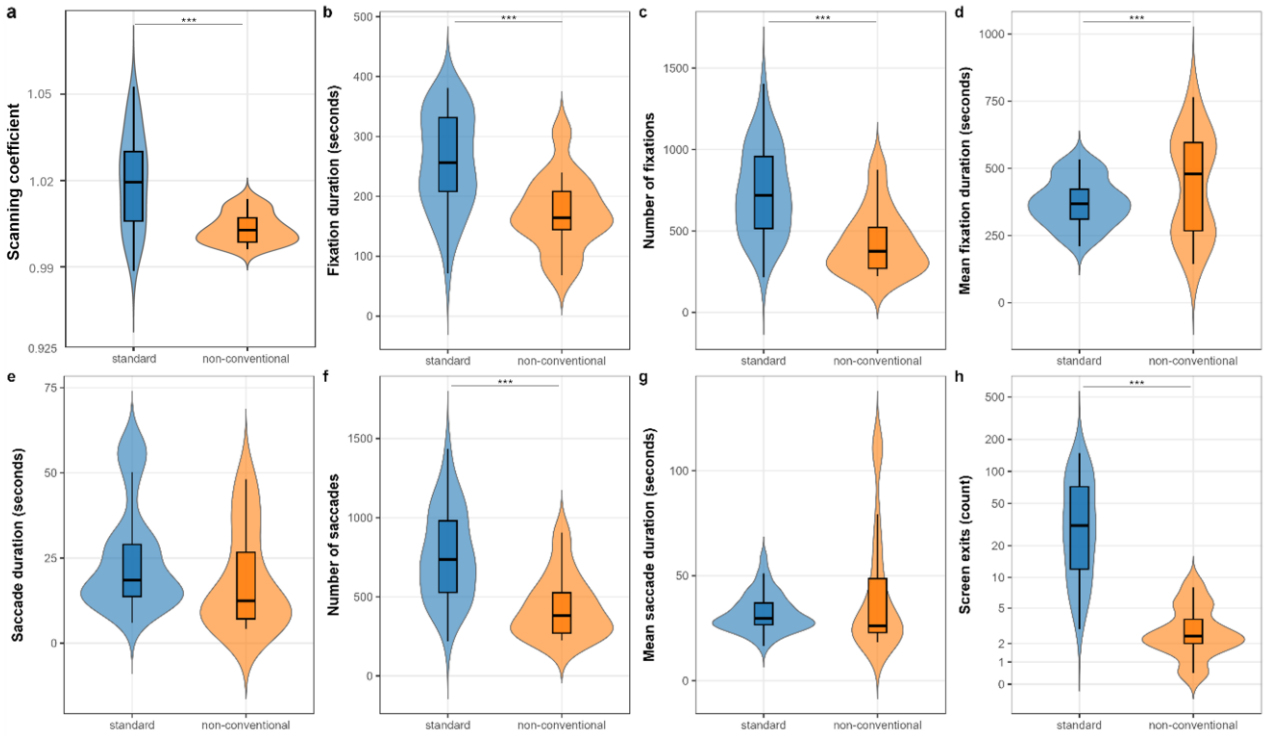


Fig. 2 Distribution of eye-tracking parameters in physicians using their usual device**:** standard mouse users with the standard mouse (blue) and non-conventional mouse users with the non-conventional mouse (orange), shown as violin plots with embedded box plots. Upper bars indicate significant differences according to the mixed model adjustment (***: $p < 0.001$).

Finally, to assess the impact of examination complexity on device performance, a mixed model analysis was conducted across three groups: normal, few lesions, and multi-lesional examinations. As illustrated in Figure 3, most eye-tracking parameters, including number and duration of fixations, number and duration of saccades, and mean total durations, showed no significant difference between the two devices ($p > 0.05$). However, two notable effects of the device were observed: the number of gaze exits was reduced with the non-conventional

mouse, both in few-lesion and multi-lesional cases. In addition, the total examination time was significantly shorter with the non-conventional device in multi-lesional cases.

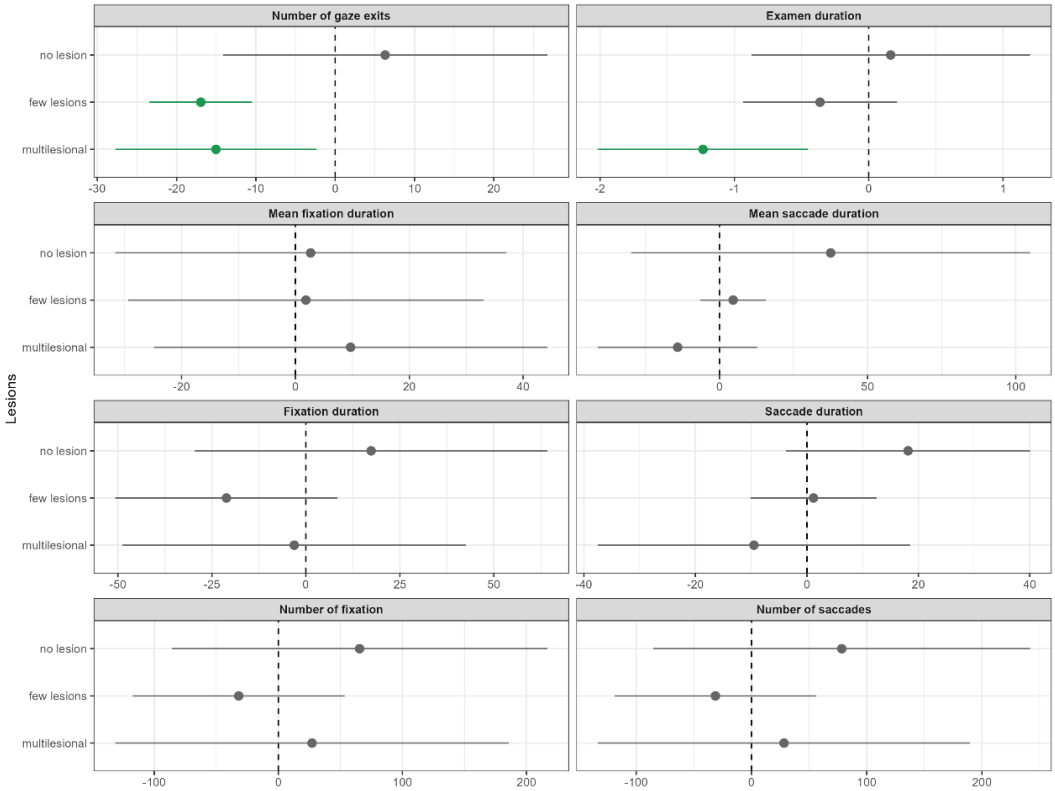


Fig. 3 Mean differences in eye-tracking parameters between standard and non-conventional mice shown for each lesion subgroup, estimated using β coefficients from linear models adjusted for physician and examination duration. Dots represent the estimated β values, with negative values indicating lower parameter values when using the non-conventional mouse. Horizontal bars correspond to 95% confidence intervals, and green dots denote statistically significant differences ($p < 0.05$).

2. Time analysis

Examination duration tended to be shorter with the non-conventional mouse in the overall cohort (4min18s vs. 4min51s; p = 0.125). In subgroup analyses, this difference was significant among physicians accustomed to using a non-conventional mouse (3min03s vs. 4min08s min; p = 0.031), but not among those accustomed to a standard mouse (5min07s vs. 5min20s; p = 0.576).

3. Mouse Kinematics and Shortcuts

A significant reduction in both maximum and average mouse movement speed, as well as in the total distance travelled, was observed with the non-conventional mouse compared to the standard mouse (Fig. **4**). In contrast, no significant differences were found in the total number of movements or in the frequency of unintended movements (defined as displacements < 5 px).

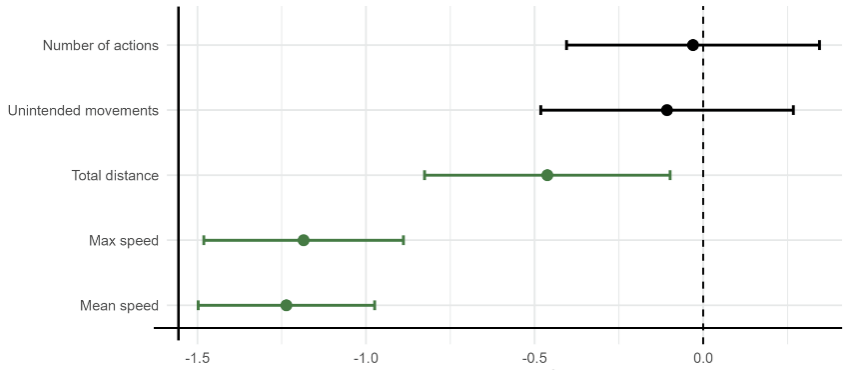


Fig. 4 Effect of the device (standard vs. non-conventional mouse) on movement parameters, expressed as standardized β coefficients (95% CI) derived from mixed models adjusted for physician and usual device.

A significant reduction in the number of shortcuts used was observed with the non-conventional mouse compared to the standard mouse. This difference involved not only windowing changes (F5 to F8 keys) but also the use of distance and metabolic intensity measurement tools, as well as the number of right and left clicks (Table IV)

Table IV Comparison of shortcut use between the non-conventional and standard mouse, using the Wilcoxon test. Values represent the median across all physicians for each device.

Category	**Median (Non-Conventional Mouse)**	**Median (Standard Mouse)**	***p-value***
Left Click Down	171 (±130)	213 (±135)	**0.0129**
Right Click Down	114 (±73.2)	169 (±116)	**0.0380**
Touches F (F5–F8)	35 (±12.1)	49 (±18.5)	**0.0129**
Touches V + D	27 (±15.9)	42 (±16.1)	0.0571

4. Qualitative analysis

The comparative analysis of qualitative analysis parameters is presented Fig. **5**. The qualitative analysis showed that the mean score of all evaluated parameters was higher for the non-conventional mouse than for the standard mouse (4.46/5 vs 3.60/5; p = 0.024). The lowest rating for the non-conventional mouse was 3.7/5 for the learning curve, whereas the lowest score for the standard mouse was 2.7/5 for ease of dictation. Other significant parameters were consistently in favor of the non-conventional mouse, including pointer fluidity, ergonomic grip, ease of handling, overall preference and performance, time efficiency, and ease of dictation. In contrast, cognitive load, learning curve, haptic feedback, and overall performance and efficiency were rated similarly between the two devices, with no observed significant differences.

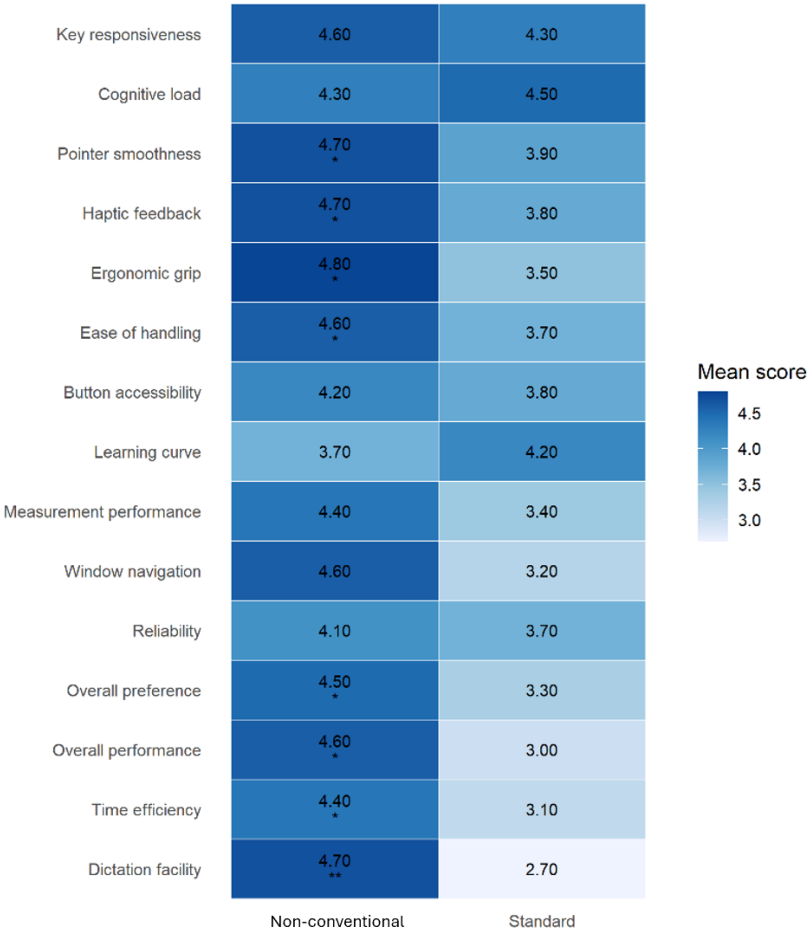


Fig. 5 Mean likerts scores and standard deviation of qualitative analysis by criterion according to mouse type (non-conventional vs. standard). Asterisks indicate significant differences after Benjamini–Hochberg correction (paired Wilcoxon test).

Concerning overall satisfaction with the two devices before and after the study, an increase in the number of dissatisfied physicians was observed for the standard mouse. Conversely, for the non-conventional mouse, a substantial proportion of physicians who were initially neutral reported high satisfaction after testing the device during the study (Figure 6).

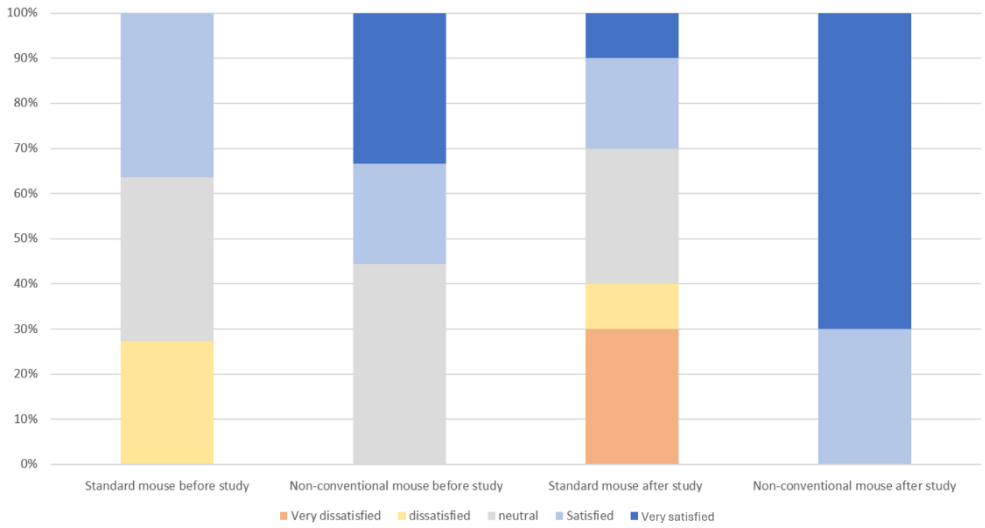


Figure 6 Physicians' satisfaction with the standard and non-conventional mouse, before and after the study.

DISCUSSION

This prospective, multicenter study is the first to assess ergonomics in nuclear medicine through a combined objective and qualitative approach, integrating eye-tracking technology as an innovative tool to explore visual behavior during image interpretation. Our findings demonstrate that the use of a non-conventional mouse positively influences eye-tracking patterns during image interpretation, mouse movement kinematics, the accuracy of executed commands, and overall work quality. These effects were more pronounced in physicians' established habits with the non-conventional device. They were only minimally influenced by examination complexity, except for a reduction in the number of screen exits and in interpretation time, both in favor of the non-conventional mouse.

Regarding the definition of eye-tracking parameters, a fixation corresponds to the momentary pause of the gaze on a point of interest, enabling its cognitive integration and contributing to a clinical decision (e.g., recognition of an abnormality, refinement of the diagnosis, or identification of an artifact). In contrast, a saccade represents an active search phase, characterized by rapid and continuous eye movements scanning the screen for relevant information (28,31,32). Some previous studies comparing experts and novices have shown that experts tend to perform shorter saccades (33), whereas others have reported the opposite trend, with an increase in saccade duration (34) and a reduction in their number (29,35), reflecting either more efficient information scanning and faster visual selection. This behavior may indicate reduced visual fragmentation and a more continuous exploration of relevant areas rather than frequent shifts of attention. Similarly, fixation duration decreases among experts, reflecting faster and less redundant focusing on the area of interest (27,30,36,37). This effect has been confirmed in other medical domains (Brunyé et al., in cardiology: experts exhibited ~691 ± 352 fixations compared with ~1359 ± 513 in novices, representing a ~49% reduction) (29,38). Applied to our study, our results suggest that the non-conventional mouse promotes

a strategy close to that of experienced physicians: fewer overall fixations but likely longer and more focused ones on relevant areas facilitated by optimized equipment, because all lesions were well analyzed by each physician despite these pattern modifications. The reduction in screen exits during complex cases reflects improved visual focus with longer but fewer saccades. This interpretative quality is further supported by the absence of visual cues required on the keyboard, the increased precision of the pointing device, and the accessibility of shortcuts. Together, these factors reduce the simultaneous management of multiple tasks (microphone, keyboard, mouse) which represent a source of interruptions and errors (+12% error rate during task interruptions in radiology reported by Balint BJ et al.(39)), and reduce disorganization as well as unnecessary prolongation of the interpretation process (24,40). The average fixation duration, which was similar between the two devices, was expected in our cohort of nuclear medicine specialists and is consistent with findings reported in the literature (33).

In our study, the use of a non-conventional mouse was associated with a significant reduction in mean speed, maximum speed, and total distance travelled. Milisavljevic et al. [22] reported that a more active exploration task increased both the time spent moving the mouse (23.3% vs. 18.9%, $p < 0.001$) and the number of movements performed (6.77 vs. 5.43, $p < 0.001$). Accordingly, the reduction in kinematic parameters may reflect a lighter cognitive load with the non-conventional mouse, facilitating examination review. These findings align with prior studies establishing a direct link between mouse kinematics and cognitive processes [23]. The decreases in mean and maximum speed and in distance travelled suggest more controlled navigation and fewer parasitic movements. Furthermore, standard kinematic analyses show that mouse trajectories are inherently composed of multiple correction cycles, spend more than 70% of their duration in deceleration, and are influenced by the use of specialized pointing devices [24].

The qualitative feedback confirmed a strong preference for the non-conventional mouse, attributed to its ergonomics, efficiency, and the ability to dictate while interpreting. Designed for intensive use, it was considered overall more pleasant than a standard office mouse, likely due to more sensitive buttons, a larger scroll wheel, and greater robustness. Although the learning curve was perceived as less favorable, this was most likely due to the need to memorize button functions and the unusual thumb movements required to access shortcuts. This constraint was addressed in our protocol by requiring participants to complete more than 20 hours of adaptation with both devices before study inclusion. Despite the presumed difficulty in precisely operating the shortcuts of the non-conventional mouse, the number of commands executed with the standard device remained markedly higher, suggesting greater precision with the optimized mouse. Therefore, it seems important that mouse button programming follows a logical layout, for example grouping windowing, measurement, and capture functions coherently, with the most frequently used commands assigned to the most accessible buttons. These results are consistent with the study by K. Denton [3], which reported a strong preference for the non-conventional mouse by radiologists, considered more efficient (66.1%), requiring less time (62.7%) and effort (74.6%) for image viewing, facilitating windowing manipulation (76.3%), and providing greater user comfort (78.0%). In our cohort, which was predominantly unfamiliar with this type of device, satisfaction increased from a neutral position to near-complete acceptance, exceeding the 83% satisfaction reported by Denton et al [3] for the non-conventional mouse (vs. 36% for the standard mouse). Other studies have similarly confirmed physicians' preference for specialized pointing devices (trackballs, tablets, and jog shuttles) over standard equipment [6,7].

This study has several limitations, the most important being the small sample size of physicians included, which limits its statistical power. Nevertheless, its multicenter design, involving institutions of different types (university hospital, cancer center, peripheral hospital, and private center), strengthens the representativeness of the findings. Another limitation is the

evaluation of a single device, without comparison with other pointing devices such as trackballs, although this choice was justified by the routine use of this mouse in two participating centers. The relatively short duration of the sessions and the sequence of examinations may also have introduced a learning effect, which we attempted to minimize by requiring a 20-hour adaptation period and by randomizing both the device used and the order of examinations. Larger studies comparing different devices are needed to assess their impact on diagnostic accuracy. The impact on reproducibility and the potential modification of metabolic or morphological measurements was not assessed in this study and may be investigated in future research.

This first study assessing ergonomics in medical imaging through eye tracking demonstrates that a dedicated device can both optimize interpretation efficiency and significantly enhance physicians' working experience.

CONCLUSION

In this prospective multicenter study, we demonstrate for the first time in nuclear medicine the value of an optimized pointing device for image interpretation, using a unique quantitative approach that combines eye tracking and mouse movement analysis.

BIBLIOGRAPHY

1. Guignard R, Cimarelli S, Fernandez V, Geffroy B. Dynamique de l'innovation en médecine nucléaire : une décennie propice pour la diffusion de la TEP. Médecine Nucléaire. juill 2021;45(4):206.

2. Katsari K, Penna D, Arena V, Polverari G, Ianniello A, Italiano D, et al. Artificial intelligence for reduced dose 18F-FDG PET examinations: a real-world deployment through a standardized framework and business case assessment. EJNMMI Phys. déc 2021;8(1):25.

3. Koopman D, Van Dalen JornA, Stevens H, Slump CH, Knollema S, Jager PL. Performance of Digital PET Compared with High-Resolution Conventional PET in Patients with Cancer. J Nucl Med. oct 2020;61(10):1448-54.

4. Teoh EJ, McGowan DR, Macpherson RE, Bradley KM, Gleeson FV. Phantom and Clinical Evaluation of the Bayesian Penalized Likelihood Reconstruction Algorithm Q.Clear on an LYSO PET/CT System. J Nucl Med. sept 2015;56(9):1447-52.

5. Ruan W, Qin C, Liu F, Pi R, Gai Y, Liu Q, et al. Q.Clear reconstruction for reducing the scanning time for 68 Ga-DOTA-FAPI-04 PET/MR imaging. Eur J Nucl Med Mol Imaging. juin 2023;50(7):1851-60.

6. Weyts K, Lasnon C, Ciappuccini R, Lequesne J, Corroyer-Dulmont A, Quak E, et al. Artificial intelligence-based PET denoising could allow a two-fold reduction in [18F]FDG PET acquisition time in digital PET/CT. Eur J Nucl Med Mol Imaging. sept 2022;49(11):3750-60.

7. Xu J, Gong E, Pauly J, Zaharchuk G. 200x Low-dose PET Reconstruction using Deep Learning [Internet]. arXiv; 2017 [cité 30 déc 2023]. Disponible sur: http://arxiv.org/abs/1712.04119

8. Margail C, Merlin C, Billoux T, Wallaert M, Otman H, Sas N, et al. Imaging quality of an artificial intelligence denoising algorithm: validation in 68Ga PSMA-11 PET for patients with biochemical recurrence of prostate cancer. EJNMMI Res. 25 mai 2023;13(1):50.

9. Muzaffar R, Christopher K, Frye R, Sterkel B, Gandhi H, Gulaka P, et al. Impact of AI on Image Quality and SUV Quantification on F18-FDG PET/CT . J Nucl Med. 1 mai 2020;61(supplement 1):1479.

10. Bonardel G, Dupont A, Decazes P, Queneau M, Modzelewski R, Coulot J, et al. Clinical and phantom validation of a deep learning based denoising algorithm for F-18-FDG PET images from lower detection counting in comparison with the standard acquisition. EJNMMI Phys. déc 2022;9(1):36.

11. Burton C. SubtlePET Analysis Using American College of Radiology Phantom and Guidelines. J Nucl Med. 1 août 2022;63(supplement 2):3290.

12. De Summa M, Ruggiero MR, Spinosa S, Iachetti G, Esposito S, Annunziata S, et al. Denoising approaches by SubtlePET™ artificial intelligence in positron emission tomography (PET) for clinical routine application. Clinical and Translational Imaging. 2024;1-10.

13. Carles M, Fechter T, Martí-Bonmatí L, Baltas D, Mix M. Experimental phantom evaluation to identify robust positron emission tomography (PET) radiomic features. EJNMMI Phys. déc 2021;8(1):46.

14. Pfaehler E, Beukinga RJ, De Jong JR, Slart RHJA, Slump CH, Dierckx RAJO, et al. Repeatability of ^{18} F- FDG PET radiomic features: A phantom study to explore sensitivity to image reconstruction settings, noise, and delineation method. Medical Physics. févr 2019;46(2):665-78.

15. Vallières M, Zwanenburg A, Badic B, Cheze Le Rest C, Visvikis D, Hatt M. Responsible Radiomics Research for Faster Clinical Translation. J Nucl Med. févr 2018;59(2):189-93.

16. Nioche C, Orlhac F, Boughdad S, Reuzé S, Goya-Outi J, Robert C, et al. LIFEx: A Freeware for Radiomic Feature Calculation in Multimodality Imaging to Accelerate Advances in the Characterization of Tumor Heterogeneity. Cancer Research. 15 août 2018;78(16):4786-9.

17. Le V, Frye S, Botkin C, Christopher K, Gulaka P, Sterkel B, et al. Effect of PET Scan with Count Reduction Using AI-Based Processing Techniques on Image Quality. J Nucl Med. 1 mai 2020;61(supplement 1):3095.

18. Jaudet C, Weyts K, Lechervy A, Batalla A, Bardet S, Corroyer-Dulmont A. The Impact of Artificial Intelligence CNN Based Denoising on FDG PET Radiomics. Front Oncol. 24 août 2021;11:692973.

19. Lovinfosse P, Visvikis D, Hustinx R, Hatt M. FDG PET radiomics: a review of the methodological aspects. Clin Transl Imaging. oct 2018;6(5):379-91.

20. Hricak H, Ward ZJ, Atun R, Abdel-Wahab M, Muellner A, Scott AM. Increasing Access to Imaging for Addressing the Global Cancer Epidemic. Radiology. déc 2021;301(3):543-6.

21. NHS England. Diagnostic Imaging Dataset 2020–21 Data. NHS England; 2021.

22. Denton K, Haider I, Hill J, Hunt SL, Ash R. Of Mice and Roentgen: Radiologist Satisfaction with a Non-conventional 13-Button Mouse—One Institution’s Experience. J Digit Imaging. déc 2018;31(6):776-82.

23. Siemens Healthineers. syngo.via WebViewer Operator Manual – Web Client VA20B [Internet]. Siemens Healthineer; 2020. Disponible sur: https://doclib.siemens-healthineers.com/rest/v1/view?document-id=781320&utm_source=chatgpt.com

24. Drew T, Williams LH, Aldred B, Heilbrun ME, Minoshima S. Quantifying the costs of interruption during diagnostic radiology interpretation using mobile eye-tracking glasses. J Med Imag. 2 mars 2018;5(03):1.

25. Lidén M, Andersson T, Geijer H. Alternative User Interface Devices for Improved Navigation of CT Datasets. J Digit Imaging. févr 2011;24(1):126-34.

26. Sherbondy AJ, Holmlund D, Rubin GD, Schraedley PK, Winograd T, Napel S. Alternative Input Devices for Efficient Navigation of Large CT Angiography Data Sets. Radiology. févr 2005;234(2):391-8.

27. Gegenfurtner A, Lehtinen E, Säljö R. Expertise Differences in the Comprehension of Visualizations: a Meta-Analysis of Eye-Tracking Research in Professional Domains. Educ Psychol Rev. déc 2011;23(4):523-52.

28. Brunyé TT, Drew T, Weaver DL, Elmore JG. A review of eye tracking for understanding and improving diagnostic interpretation. Cogn Research. déc 2019;4(1):7.

29. Brunyé TT, Nallamothu BK, Elmore JG. Eye-tracking for assessing medical image interpretation: A pilot feasibility study comparing novice vs expert cardiologists. Perspect Med Educ. 11 avr 2019;8(2):65-73.

30. Borys M, Plechawska-Wójcik M. Eye-tracking metrics in perception and visual attention research. EJMT. 2017;3:11-23.

31. Rayner K. Eye movements in reading and information processing: 20 years of research. Psychological Bulletin. 1998;124(3):372-422.

32. Leveque L, Bosmans H, Cockmartin L, Liu H. State of the Art: Eye-Tracking Studies in Medical Imaging. IEEE Access. 2018;6:37023-34.

33. Bertram R, Kaakinen J, Bensch F, Helle L, Lantto E, Niemi P, et al. Eye Movements of Radiologists Reflect Expertise in CT Study Interpretation: A Potential Tool to Measure Resident Development. Radiology. déc 2016;281(3):805-15.

34. Gegenfurtner A, Lehtinen E, Säljö R. Expertise Differences in the Comprehension of Visualizations: a Meta-Analysis of Eye-Tracking Research in Professional Domains. Educ Psychol Rev. déc 2011;23(4):523-52.

35. Ji Y, Kong Z, Deng Y, Chen J, Liu Y, Zhao L. The role of eye tracker in teaching video-assisted thoracoscopic surgery: the differences in visual strategies between novice and expert surgeons in thoracoscopic surgery. Ann Transl Med. mai 2022;10(10):592-592.

36. Waite S, Kolla S, Jeudy J, Legasto A, Macknik SL, Martinez-Conde S, et al. Tired in the Reading Room: The Influence of Fatigue in Radiology. Journal of the American College of Radiology. févr 2017;14(2):191-7.

37. Donovan T, Litchfield D. Looking for Cancer: Expertise Related Differences in Searching and Decision Making. Applied Cognitive Psychology. janv 2013;27(1):43-9.

38. Brunyé TT, Drew T, Kerr KF, Shucard H, Weaver DL, Elmore JG. Eye tracking reveals expertise-related differences in the time-course of medical image inspection and diagnosis. J Med Imag [Internet]. 27 oct 2020 [cité 17 sept 2025];7(05). Disponible sur: https://www.spiedigitallibrary.org/journals/journal-of-medical-imaging/volume-7/issue-05/051203/Eye-tracking-reveals-expertise-related-differences-in-the-time-course/10.1117/1.JMI.7.5.051203.full

39. Balint BJ, Steenburg SD, Lin H, Shen C, Steele JL, Gunderman RB. Do Telephone Call Interruptions Have an Impact on Radiology Resident Diagnostic Accuracy? Academic Radiology. déc 2014;21(12):1623-8.

40. Wynn RM, Howe JL, Kelahan LC, Fong A, Filice RW, Ratwani RM. The Impact of Interruptions on Chest Radiograph Interpretation. Academic Radiology. déc 2018;25(12):1515-20.

GENERAL CONCLUSION

This work provides an original contribution to ergonomics in nuclear imaging by integrating image quality optimisation (reduced acquisition time and noise reduction through artificial intelligence) with the optimisation of image manipulation (non-conventionnal pointing device, eye-tracking, and mouse kinematic analysis).

We evaluated two tools that remain rarely used in clinical practice: the first artificial intelligence software specifically dedicated to nuclear medicine, and a non-conventional mouse originally designed for the video gaming domain.

In accordance with the definition of ergonomics, we have enriched the existing literature with new data derived from a methodological evaluation of these tools, designed to enhance overall system performance and optimise physicians' well-being in their interpretative tasks. This approach underlines the importance of conducting an initial and continuous evaluation of any medical device, where diagnostic quality directly determines therapeutic management. Each link in the diagnostic chain, from the acquisition device to the interpretation mouse, must therefore be integrated into an evidence-based medicine framework, irrespective of commercial claims or prior use in other contexts. In a technically demanding medical specialty such as nuclear medicine, a thorough understanding of this chain remains essential to ensure full control of information and guarantee its reliability. The rapid rise of artificial intelligence, based on neural networks trained on defined populations, confronts us with a tool whose internal functioning remains largely opaque, and whose results rely on multiple weight adjustments carried out autonomously, without any possibility of user control.

In parallel, image interaction devices have evolved more slowly than acquisition and reconstruction systems, leading to the use of peripherals originally developed for other purposes (notably gaming), whose clinical validity remains to be established.

To evaluate these two devices as comprehensively as possible, we adopted a multi-step

approach, beginning with a preclinical assessment. The SubtlePET® software was tested on a phantom, confirming a reduction in background noise variability and an expected decrease in metabolic values, while also highlighting its main limitation: the inability to recover a signal absent from the reconstructed images (explained by the lack of access to the raw sinogram data). This preclinical phase was not necessary for the non-conventionnal mouse, already in use at Le Mans Hospital and by several physicians at Angers University Hospital, demonstrating its prior clinical interest.

Quantitative evaluation confirmed the relevance of these tools: radiomic analysis demonstrated excellent preservation of the extracted features, despite the known sensitivity of these parameters to acquisition and reconstruction conditions. The eye-tracking assessment of the non-conventionnal mouse revealed an improvement in visual exploration patterns, reflected by a reduction in the duration and number of fixations and saccades, suggesting a potential gain in diagnostic efficiency. This effect was further enhanced among physicians already familiar with the device. Other parameters, such as kinematics and shortcut-use accuracy, also showed improvement.

Finally, qualitative and subjective evaluation highlighted an overall improvement in the quality of denoised images compared with those obtained by reducing acquisition time without denoising. However, physicians' confidence remained limited, due to altered image appearance and the emergence or exacerbation of some artefacts. Regarding the mouse, a clear preference was expressed in favour of the non-conventional device across most criteria (ergonomics, usability, and efficiency), along with a stated willingness to shift from a standard mouse to this type of peripheral.

Furthermore, although the economic impact has not been directly studied, certain implications can be deduced. The use of SubtlePET® software reduces examination time, thereby potentially increasing the number of patients per shift or reducing the dose of radiotracer injected, contributing to lower radiopharmaceutical costs. *Katsari et al (2021)* confirm this

observation, with savings on radiotracers more than offsetting the cost of using SubtlePET® software. For its part, the non-conventional mouse would reduce interpretation time, potentially also improving overall efficiency. In addition, its robust design, adapted for intensive use, meets a requirement for durability that is often lacking in current devices. The commercial cost of using the SubtlePET® software and purchasing non-conventionnal mice remains to be deducted from this potential gain.

This work therefore underscores the importance of systematically evaluating any tool that may directly or indirectly influence the interpretative task in nuclear medicine. It highlights the benefits of integrating specialised and well-adapted technological solutions, whether reconstruction software or interaction peripherals.

Ultimately, the combination of robust artificial intelligence algorithms with interfaces designed for experts could establish a new quality standard, where scientific rigor meets ergonomic requirements, to the benefit of both physicians and patients.

Article 1

Clinical value of artificial intelligence in reducing pet image acquisition time: routine clinical validation using qualitative, quantitative, and radiomic analysis on a cohort of 282 patients undergoing [^{18}F]FDG and [^{68}Ga]PSMA PET/CT

LIST OF FIGURES

Figure 1 : Acquisition of a NEMA phantom ..... Page 21

Figure 2 : Background noise variability ..... Page 22

Figure 3 : Flow chart of patient ..... Page 23

Figure 4 : PCA of qualitative scores ..... Page 25

Figure 5 : Alluvial charts of scores [^{18}F]FDG radiotracer ..... Page 26

Figure 6 : Alluvial charts of scores [^{68}Ga]PSMA radiotracer ..... Page 27

Figure 7 : Focal hypermetabolism and overlap margin artefacts ..... Page 28

Figure 8 : CCC of radiomic features extracted from [^{18}F]FDG and [^{68}Ga]PSMA ..... Page 31

Figure 9 : Number of radiomic features with CCC < 0.8 ..... Page 32

Resource 1 : Variation of sphere-to-background contrast ..... Page 43

Resource 2 : CCC for all radiomics features extracted ..... Page 44

LIST OF TABLES

Table I : Baseline characteristics of the study population ..... Page 24

Table II : PCA loadings of qualitative parameters (appendix) ..... Page 41

Table III : Comparison of reconstruction methods – [^{18}F]FDG ..... Page 27

Table IV : Comparison of reconstruction methods – [^{68}Ga]PSMA ..... Page 28

Table V : Confidence in presence of significant hypermetabolism ..... Page 29

Table VI : SUVmax values – [^{18}F]FDG ..... Page 30

Table VII : SUVmax values – [^{68}Ga]PSMA ..... Page 30

Table VIII : SUVmax variability and reproducibility metrics (appendix) ..... Page 41

Table IX : Most impacted radiomic characteristics (CCC < 0.8) ..... Page 33

Table X Radiomic characteristics (CCC < 0.8) only for [18F]FDG ..... Page 34

Table XI Radiomic characteristics (CCC < 0.8) only for [^{68}Ga]PSMA ..... Page 34

Article 2

Innovative evaluation of a non-conventional mouse for image interpretation in metabolic imaging: integration of eye tracking, kinematic analysis, and qualitative feedback

LIST OF FIGURES

Figure 1 : Schematic representation of a non-conventional mouse..... Page 50

Figure 2 : Eye-tracking parameters in physicians using their usual device..... Page 56

Figure 3 : Influence of the number of lesion on eye-tracking parameters..... Page 57

Figure 4 : Effect of the device on movement parameters.....Page 58

Figure 5 : likerts scores and standard deviation of qualitative analysis.....Page 59

Figure 6 : Physicians' satisfaction with the standard and non-conventional mouse.....Page 60

LIST OF TABLES

Table I : Keyboard and non-conventional mouse shortcuts..... Page 50

Table II : Demographic, professional, and practice-related characteristics ..... Page 54

Table III : Comparison of eye-tracking parameters..... Page 55

Table IV : Comparison of shortcut use..... Page 58

TABLE DES MATIERES

SERMENT D'HIPPOCRATE ..... D
TABLE DES MATIERES 6
GENERAL INTRODUCTION 8

CLINICAL VALUE OF ARTIFICIAL INTELLIGENCE IN REDUCING PET IMAGE ACQUISITION TIME: ROUTINE CLINICAL VALIDATION USING QUALITATIVE, QUANTITATIVE, AND RADIOMIC ANALYSIS ON A COHORT OF 282 PATIENTS UNDERGOING [^{18}F]FDG AND [^{68}GA]PSMA PET/CT 12
ABSTRACT 13
INTRODUCTION 14
MATERIALS AND METHODS 16
1. Clinical population 16
2. Image acquisition and processing 16
3. SubtlePET® algorithm 17
4. Phantom acquisition 18
5. Image quality and quantitative analysis 18
6. Statistical analysis 19

RESULTS 21
1. Phantom analysis 21
2. Clinical analysis 22
2.1. Population 22
2.2. Qualitative analysis 24
2.3. Subgroup analysis 29
2.4. Semi-quantitative analysis 29
3. Radiomics analysis 31

DISCUSSION 35
CONCLUSION 39
BIBLIOGRAPHY 40
SUPPLEMENTARY INFORMATION 43
ONLINE RESOURCE 44

INNOVATIVE EVALUATION OF A NON-CONVENTIONAL MOUSE FOR IMAGE INTERPRETATION IN METABOLIC IMAGING: INTEGRATION OF EYE TRACKING, KINEMATIC ANALYSIS, AND QUALITATIVE FEEDBACK 46
ABSTRACT 47
INTRODUCTION 48

MATERIALS AND METHODS **50**
1. Medical study population **50**
2. Materials **50**
2.1. Computer mouse 50
2.2. Eye Tracker 52
3. Quantitative measures **52**
3.1. Study protocol 52
3.2. Eye-tracking analysis 53
3.3. Time analysis 53
3.4. Mouse Movement Analysis 53
4. Qualitative Parameters **54**
5. Statistical Analysis **54**
RESULTS **55**
1. Eye-tracking Analysis **55**
2. Time analysis **58**
3. Mouse Kinematics and Shortcuts **59**
4. Qualitative analysis **60**
DISCUSSION **62**
CONCLUSION **66**
BIBLIOGRAPHY **67**

GENERAL CONCLUSION **71**
TABLE DES MATIERES **76**

DAMBRAIN Abel

Ergonomics and Artificial Intelligence in PET Imaging: Impact of User Interfaces on Diagnostic Performance

Introduction In nuclear medicine, diagnostic improvement cannot be limited to technological advances; interpretation interfaces are also a major challenge. This study evaluates SubtlePET® and an alternative mouse to optimise image quality and physicians' working conditions. **Methods** SubtlePET® was first assessed on a phantom study to characterise the parameters required for clinical translation, and then applied to a cohort of 285 PET examinations ([^{18}F]FDG, [^{68}Ga]PSMA) reconstructed under standard conditions (R100), with reduced acquisition times (R75, R50), and after denoising (S75, S50). Metabolic and radiomic data were extracted and compared. For the alternative mouse, 10 physicians each interpreted 14 examinations using both a standard and the new device. Oculographic patterns, together with temporal and kinematic data, were analysed. Finally, a qualitative assessment based on standardised questionnaires gathered physicians' perceptions of ease of use, visual rendering, and acceptability of the tools tested. **Results** The phantom study revealed no difference in contrast but demonstrated reduced noise variability and preservation of radiomic parameters. In clinical practice, [^{18}F]FDG images showed improvements in S75 denoised reconstructions for all criteria except diagnostic confidence. For [^{68}Ga]PSMA, only hepatic parenchyma quality was significantly impaired in S50 images. SUVmax decreased in denoised images (−7.73% for [^{18}F]FDG; −11.46% for [^{68}Ga]PSMA, $p < 0.0001$), while 90% of radiomic parameters remained strongly correlated (CCC > 0.8). With the alternative mouse, the number of fixations (571 vs 635; $p = 0.004$), their total duration (220 vs 242 s; $p = 0.035$), and saccades ($p < 0.01$) decreased, as did movement speed and distance travelled ($p < 0.05$). The number of executed shortcuts was reduced, and ease of interpretation was rated higher (4.5/5 vs 3.6/5; $p = 0.02$). **Conclusion** These two studies demonstrate that innovations in artificial intelligence and user interfaces act as complementary levers to simultaneously improve physicians' working conditions and the quality of nuclear medicine examinations.

Keywords : Artificial intelligence, ergonomics, mouse, SubtlePET, PET

Ergonomie et intelligence artificielle en imagerie TEP : Impact des interfaces utilisateur sur la performance diagnostique

Introduction En médecine nucléaire, l'amélioration diagnostique ne peut se limiter aux avancées technologiques : les interfaces d'interprétation sont un enjeu majeur. Cette étude évalue SubtlePET® et une souris non conventionnelle pour optimiser la qualité des images et les conditions de travail. **Méthodes** Le logiciel SubtlePET® a été évalué initialement sur fantôme, permettant de caractériser les paramètres nécessaires à sa transposition clinique, puis sur une cohorte de 285 examens TEP ([^{18}F]FDG, [^{68}Ga]PSMA) reconstruits en condition standard (R100), avec réduction du temps (R75, R50) et après débruitage (S75, S50). Les données métaboliques et radiomiques furent extraites et comparées. Concernant la souris non conventionnelle, 10 médecins interprétèrent 14 examens avec une souris standard et innovante. Les patterns oculographiques ainsi que les données temporelles et cinématiques furent analysées. Enfin, une évaluation qualitative, reposant sur des questionnaires standardisés, a recueilli les perceptions des médecins quant au confort d'utilisation, au rendu visuel et à l'acceptabilité des outils testés. **Résultats** L'étude sur fantôme n'a montré aucune différence de contraste, mais une réduction de la variabilité du bruit et une préservation des paramètres radiomiques. En clinique, les images en [^{18}F]FDG montraient une amélioration des images débruités S75 sur tous les critères mis à part la confiance diagnostic. En [^{68}Ga]PSMA, seule la qualité du parenchyme hépatique était jugée altérée. Une diminution du SUVmax était observée mais 90 % des paramètres radiomiques restaient fortement corrélés (CCC > 0,8). Avec la souris non conventionnelle, le nombre de fixations (571 vs 635 ; $p = 0,004$), leur durée totale (220 vs 242 s ; $p = 0,035$) et les saccades ($p < 0,01$) diminuaient, de même que la vitesse et la distance parcourue ($p < 0,05$) avec la souris. Le nombre de raccourcis exécutés était réduit et le confort d'interprétation était jugé supérieur (4,5/5 vs 3,6/5 ; $p = 0,02$). **Conclusion** Ces deux études démontrent que l'innovation ergonomique et l'intelligence artificielle constituent des leviers complémentaires pour optimiser à la fois les conditions de travail des médecins et la qualité des examens en médecine nucléaire.

Mots clefs : Intelligence artificielle, ergonomie, souris, SubtlePET, PET